Importance of Aerosol Composition and Aerosol Vertical Profile in Global Spatial Variation ~~in~~ of the $PM_{2.5}$ to AOD Relationship ~~Strongly Influenced by Aerosol Composition~~

Haihui Zhu[1]*, Randall V. Martin[1], Aaron van Donkelaar[1], Melanie S. Hammer[1], Chi Li[1], Jun Meng[2], Christopher R. Oxford[1], Xuan Liu[1], Yanshun Li[1], Dandan Zhang[1], Inderjeet Singh[1], Alexei Lyapustin[3]

[1]Department of Energy, Environmental & Chemical Engineering, Washington University in St. Louis, St. Louis, MO, USA

[2]Department of Civil and Environmental Engineering, Washington State University, Pullman, WA, USA

[3]Laboratory for Atmospheres, NASA Goddard Space Flight Center, Greenbelt, MD, USA

Correspondence: Haihui Zhu (haihuizhu@wustl.edu)

Abstract Ambient fine particulate matter ($PM_{2.5}$) is the leading global environmental determinant of mortality. However, large gaps exist in ground-based $PM_{2.5}$ monitoring. Satellite remote sensing of aerosol optical depth (AOD) offers information to fill these gaps worldwide, when augmented with a modeled $PM_{2.5}$ to AOD relationship ~~(η)~~. This study aims to understand the spatial pattern and driving factors of ~~η~~ the relationship by examining η ($=\frac{PM_{2.5}}{AOD}$), from both observations and modeling. A global observational estimate of η for the year 2019 is inferred from 6,~~118~~ 870 ground-based $PM_{2.5}$ measurement sites and satellite retrieved AOD ~~from the MAIAC algorithm~~. The GEOS-Chem~~A~~ global chemical transport model~~;~~ ~~GEOS-Chem,~~ in its high performance configuration (GCHP), is used to interpret the observed spatial pattern of annual mean η. Measurements and the GCHP simulation consistently identify a global population-weighted mean η of ~~92–100~~96-98 μg/m^3, with regional values ranging from ~~60.3~~59.8 μg/m^3 ~~for~~ in North America to more than ~~130~~ 190 μg/m^3 in Africa. The highest η is found in arid regions where aerosols are less hygroscopic due to mineral dust, followed by regions strongly influenced by surface aerosol sources. Relatively low η is found over regions distant from strong aerosol sources. The spatial correlation of observed η with meteorological fields, aerosol vertical profiles, and aerosol chemical composition reveals that the spatial variation of η is strongly influenced by aerosol composition ~~driven by its effects on aerosol hygroscopicity~~and aerosol vertical profile. Sensitivity tests with globally uniform parameters ~~reveal that aerosol composition leads to the strongest η spatial~~

~~variability~~quantify their effects on η spatial variability, with a population-weighted ~~normalized~~ mean difference of 12.3 μg/m^3~~,~~ for aerosol composition that ~~higher than that from aerosol vertical profile (8.4 μg/m^3),~~ reflect~~ings~~ the determinant composition effects on aerosol hygroscopicity and aerosol optical properties; and a population-weighted mean difference ~~,~~ of 8.4 μg/m^3 for aerosol vertical profile that reflects spatial variation in the column to surface relationship.

1 Introduction

Exposure to ambient fine particulate matter ($PM_{2.5}$) has been recognized as the predominant environmental risk factor for the global burden of disease, leading to millions of deaths annually (Brauer et al., 2024). Even at low $PM_{2.5}$ concentrations, long-term exposure can increase circulatory and respiratory related mortality (Christidis et al., 2019; Pinault et al., 2016; Weichenthal et al., 2022). Despite the importance of $PM_{2.5}$, many of the world's countries do not provide publicly accessible $PM_{2.5}$ data (Martin et al., 2019). Satellite remote sensing of aerosol optical depth (AOD), an optical measure of aerosol abundance, offers information about the distribution of $PM_{2.5}$ (Kondragunta et al., 2022). A large community relies upon the spatial distribution of $PM_{2.5}$ concentrations inferred from satellite AOD and a modeled $PM_{2.5}$ to AOD relationship, ~~satellite remote sensing~~ for health impact assessment and epidemiological analyses of long-term exposure (Brauer et al., 2024; Burnett et al., 2018; Cohen et al., 2017; Hao et al., 2023). Quantitative application of satellite AOD for long-term characterization of the spatial distribution of $PM_{2.5}$ would benefit from a better understanding of the factors affecting the $PM_{2.5}$-AOD relationship.

The relationship between satellite AOD and surface $PM_{2.5}$ can be established through a statistical method, a geophysical method, or their combination. A statistical method uses ground-based monitors for training and is well suited for regions with dense monitors (Di et al., 2016; Hu et al., 2014; Xin et al., 2014). A geophysical approach utilizes a chemical transport model to simulate the relationship (η) between $PM_{2.5}$ and AOD for application to satellite AOD (van Donkelaar et al., 2006, 2010; He et al., 2021), and thus depends on accurate model representation of η. V~~v~~an Donkelaar et al. (2015, 2016) combined the two methods by applying geographically weighted regression (GWR) on the geophysical $PM_{2.5}$, which further constrains geophysical $PM_{2.5}$ using ground measurements and other predictors. However, accuracy of geophysical $PM_{2.5}$ remains

critical over vast areas with sparse monitoring, and knowledge about the factors affecting η spatial variability are needed to guide improvements of modeled η and geophysical $PM_{2.5}$.

Previous studies have identified several factors that affect η variability, including aerosol vertical distribution, aerosol hygroscopicity, aerosol optical properties, and ambient meteorological factors such as relative humidity (RH), planetary boundary layer height (PBLH), wind speed, temperature, and fire events (van Donkelaar et al., 2013; Ford and Heald, 2015; Guo et al., 2017; Jin et al., 2019; Li et al., 2015; Wendt et al., 2023). Most studies focused on the temporal variability of η and found association with meteorological variables such as PBLH (Chu et al., 2015; Damascena et al., 2021; Gupta et al., 2006; He et al., 2021; Yang et al., 2019; Zhang et al., 2009). A few studies have examined the regional-scale spatial variation of η with meteorological, land type variables, and aerosol vertical profile in North America (van Donkelaar et al., 2006; Jin et al., 2020; Li et al., 2015) and China (Yang et al., 2019). To our knowledge, none have examined the factors at the global scale affecting the spatial variation of η or the effects of chemical composition.

In this work, we examine this knowledge gap about the spatial variation in η at a global scale. We first collect data from more than 6,000 $PM_{2.5}$ monitoring sites provided by ~~nine~~ ten networks and satellite AOD to obtain an observationally based map of η. We further interpret the global η distribution using the GEOS-Chem model of atmospheric composition with recent improvements in aerosol size representation, $PM_{2.5}$ diel variation, and vertical allocation. By decomposing the simulated η, we identify 2 strong drivers of η spatial variability: aerosol composition and aerosol vertical profile. We conduct sensitivity tests using GEOS-Chem to study how the two factors vary globally and how they contribute to the spatial variation in η.

2 Methods

2.1 Ground Measured $PM_{2.5}$

We collect ground-based measurements of $PM_{2.5}$ for the year 2019 ~~from which~~ to produce observational constraints on η ($\frac{PM_{2.5}}{AOD}$), the spatially and temporally varying ratio between 24-hour surface $PM_{2.5}$ concentrations and total column AOD at satellite sampling time. At the time of manuscript preparation, the year 2019 offered the greatest density of measurements and the most current emission inventory. We obtain $PM_{2.5}$ measurements from 7 regional networks and 3~~2~~

global networks, as shown in Figure A1. For the United States, we access data from the United States Environmental Protection Agency's Air Quality System (https://www.epa.gov/outdoor-air-quality-data/download-daily-data), including both Federal Reference Method and non-Federal Reference Methods $PM_{2.5}$ (e.g. IMPROVE network). $PM_{2.5}$ data for Canada are from the Environment Canada's National Air Pollution Surveillance (NAPS) program. $PM_{2.5}$ data for Europe are from the European Environment Agency Air Quality e-Reporting system (https://www.eea.europa.eu/data-and-maps/data/aqereporting). Over mainland China, $PM_{2.5}$ measurements from the National and Provincial Environmental Protection Agencies are downloaded from http://beijingair.sinaapp.com/~~, which provides instantaneous air quality data records from the National and Provincial Environmental Protection Agencies~~. Over India, $PM_{2.5}$ data are originally from the Central Pollution Control Board Continuous Ambient Air Quality Monitoring network and the U.S. embassies. Over Australia, observations are downloaded for the Northern Territory (http://ntepa.webhop.net/NTEPA/), Queensland (https://www.data.qld.gov.au/dataset/), and New South Wales (https://www.dpie. nsw.gov.au/air-quality/air-quality-data-services/data-download-facility). We require at least 5 days of measurements for each month for a monitor to be included. Additionally, we obtain $PM_{2.5}$ measurements over other regions provided by the World Health Organization (WHO) Global Ambient Air Quality Database (https://www.who.int/data/gho/data/themes/air-pollution/who-air-quality-database/2022), OpenAQ (https://openaq.org/), and ~~by~~ the Surface PARTiculate mAtter Network ~~Network~~ (SPARTAN, https://www.spartan-network.org/), which is co-located with the Aerosol Robotic Network (AERONET). SPARTAN also provides filter based $PM_{2.5}$ chemical composition, which is initially described in Snider et al., (2016). Subsequent developments to the sampling and analysis procedure of SPARTAN include an upgrade to the AirPhoton SS5 sampling station to use a cyclone inlet, an automated weighing system (MTL AH500E) to improve precision and throughput, additional black carbon analysis by Hybrid Integrating Plate/Sphere (White et al., 2016), ~~trace metal~~ elements measured by X-ray Fluorescence (Liu et al., 2024) and a global mineral dust equation (Liu et al., 2022). We require at least 50 days of coincident $PM_{2.5}$ and AERONET AOD measurements for a SPARTAN site to be included in our analysis.

We also collected publicly available $PM_{2.5}$ compositional data to assess GCHP simulated composition. Long-term $PM_{2.5}$ compositional data are included from the United States

Environmental Protection Agency's Air Quality System, the European Environment Agency Air Quality e-Reporting system, and SPARTAN, with a total of 365 sites covering the U.S. (306), Europe (37), and the Global South (22).

2.2 Satellite AOD

We obtain AOD at 550 nm from the Multi-Angle Implementation of Atmospheric Correction (MAIAC) algorithm, which offers AOD at a high spatial resolution of 1 km worldwide over both land and coastal regions (Lyapustin et al., 2018). The radiances used in the retrieval are measured by the twin MODerate resolution Imaging Spectroradiometer (MODIS) instruments onboard the Terra and Aqua satellites. Terra follows a descending orbital path, crossing the equator at 10:30 local time, while Aqua is on an ascending orbit with 13:30 equatorial crossing local time. Both MODIS instruments offer a wide swath width of 2330 km, enabling nearly global daily coverage of the Earth (Sayer et al., 2014). $PM_{2.5}$ monitoring sites with annual mean satellite AOD less than 0.05 (background AOD level over land) are excluded to reduce the influence of retrieval uncertainties on our analysis.

2.3 AERONET AOD

AERONET is a worldwide sun photometer network that provides long-term measurement of AOD. We use the Version 3 Level 2 database, which includes an improved cloud screening algorithm (Giles et al., 2019). We sample AERONET AOD within ±15 min of the satellite overpass time and interpolate to 550 nm wavelength, based on the local Ångström exponent at 440 and 670 nm. For SPARTAN sites, we sample AERONET data coincidentally with SPARTAN aerosol composition to obtain the ground-based observation of η.

2.4 GEOS-Chem Simulation

We simulate η with the GEOS-Chem chemical transport model (www.geos-chem.org, last access: 26 October 2023), driven by offline meteorological data, MERRA-2, from the Goddard Earth Observing System (GEOS) of the NASA Global Modeling and Assimilation Office (Schubert et al., 1993). We use the high-performance configuration of GEOS-Chem (GCHP) (Eastham et al., 2018) version 13.4.0 (DOI: 10.5281/zenodo.7254268), which includes advances in performance and usability (Martin et al., 2022). The simulation is conducted for the year 2019, on a C90 cubed-

sphere grid corresponding to a horizontal resolution of about 100 km, with a spin-up time of 1 month.

The GEOS-Chem aerosol simulation includes the sulfate-nitrate-ammonium (SNA) system (Fountoukis and Nenes, 2007), primary and secondary carbonaceous aerosols (Pai et al., 2020; Park et al., 2003; Wang et al., 2014), sea salt (Jaeglé et al., 2011), and natural (Fairlie et al., 2007; Meng et al., 2021) and anthropogenic (Philip et al., 2017) dust. Emissions are processed with the Harmonized Emissions Component (HEMCO) (Lin et al., 2021). The primary emission data are from the Community Emissions Data System version 2 (CEDS~~GBD-MAPS~~V2; ~~(~~Hoesly et al., 2018; CEDS, 2024) ~~McDuffie et al., 2020)~~for the year 2019. Emissions from stacks are distributed vertically (Bieser et al., 2011). Diel variation of anthropogenic emissions is included (Li et al., 2023). Resolution-dependent soil NO_x, sea salt, biogenic VOC, and natural dust emissions are calculated offline at native meteorological resolution to produce consistent emissions across resolutions (Meng et al., 2021; Weng et al., 2020). Biomass burning emissions use the Global Fire Emissions Database, version 4 (GFED4) at daily resolution (van der Werf et al., 2017) for the year 2019. We estimate organic matter (OM) from primary organic carbon using an OM/OC parameterization (Canagaratna et al., 2015; Philip et al., 2014b). For secondary aerosol components, the concentration at 2 m above the surface is used to calculate $PM_{2.5}$, following Li et al. (2023). A 50% reduction of the surface nitrate concentration is applied to account for the long-~~persisting~~ standing bias in surface nitrate simulated by GEOS-Chem (Heald et al., 2012; Miao et al., 2020; Travis et al., 2022; Zhai et al., 2021; Zhang et al., 2012~~)~~; also Figure A2~~2~~ in this manuscript) and other models~~-~~ such as CMAQ (Shimadera et al., 2014), WRF-Chem (Sha et al., 2019), and EMEP/MSC-W (Prank et al., 2016)~~(Zakoura and Pandis, 2018; Shimadera et al., 2014)~~. Despite this bias, GEOS-Chem can sufficiently represent the variability of nitrate for applications to studies at global (McDuffie et al., 2021; Weagle et al., 2018) and regional (Geng et al., 2017; Kim et al., 2015; Philip et al., 2014a; Zhai et al., 2021) scales. Dry and wet deposition follows Amos et al. (2012), with a standard resistance-in-series dry deposition scheme (Wang et al., 1998). Wet deposition includes scavenging processes from convection and large-scale precipitation (Liu et al., 2001).

Global RH-dependent aerosol optical properties are based on the Global Aerosol Data Set (GADS) (Kopke et al., 1997), as originally implemented by Martin et al. (2003), with updates for SNA and

OM dry size (Zhu et al., 2023), hygroscopicity (Latimer and Martin, 2019), mineral dust size distribution (Zhang et al., 2013), and absorbing brown carbon (Hammer et al., 2016). These updates enable GEOS-Chem to capture 74% of the AOD spatial variability versus AERONET (Zhu et al., 2023). A slight systematic low bias against MAIAC AOD is found, with an intercept of -0.05 and a population-weighted mean difference (PWMD) of -0.04. Low bias in simulated AOD is also reported for other models, such as CMAQ (Jin et al., 2019) and WRF-Chem (Benavente et al., 2023). We artificially increase simulated AOD by 0.04 globally to address this~~a~~ poorly understood systematic bias that, although minor, is useful for the representation of η (PWMD reduced from 20.6 μg/m^3 to 1.9 μg/m^3).~~.~~ $PM_{2.5}$ is calculated as the sum of each component at 35% RH to align with common measurement protocols. ~~$PM_{2.5}$ is calculated as the sum of each component at 35% RH to align with common measurement protocols.~~

2.5 Population

Global population information is obtained from the Gridded Population of the World provided by the NASA Socioeconomic Data and Applications Center (Center for International Earth Science Information Network~~ – CIESIN~~, 2018).

2.6 Sensitivity Tests with Globally Uniform Parameters

We conduct sensitivity tests of factors affecting the spatial variation of η, with a focus on aerosol composition and aerosol vertical profile. To understand the relative importance of these factors, we impose a constant for each factor and simulate the corresponding η. The difference between the test scenario and the base scenario reflects the change due to variation of the factor. We use the global population-weighted mean (PWM) and population-weighted mean difference (PWMD) to summarize changes with a focus on relevance to population exposure:

$$X_{PWM} = \frac{\sum_j \sum_i P_{i,j} X_{i,j}}{\sum_j \sum_i P_{i,j}}$$

$$PWMD = \frac{\sum_j \sum_i P_{i,j} |X_{i,j} - Y_{i,j}|}{\sum_j \sum_i P_{i,j}}$$

where i and j are grid box identifiers. X and Y could be any variable of interest. $|X_{i,j} - Y_{i,j}|$ is the absolute value of their difference. P represents population density in each grid box.

The first test imposes globally uniform aerosol chemical composition calculated as the global PWM aerosol component fraction ($F_{s,k,s,PWM}$):

$$F_{s,k,s,PWM} = \frac{\sum_j \sum_i P_{i,j} F_{i,j,s,k,s}}{\sum_j \sum_i P_{i,j}}$$

where i, j, and k are grid box identifiers along latitude, longitude, and vertical layer. ~~P represents population density in each grid box.~~ ~~Fs~~ ~~P represents population density in each grid box.~~ F_s is the fraction of aerosol component ~~S~~ s in total aerosol mass. This test keeps the total columnar aerosol mass and aerosol vertical profile unchanged.

The second test imposes a globally uniform aerosol vertical profile calculated as the PWM column relative vertical profile ($R_{s,k,s,PWM}$):

$$R_{s,k,s,PWM} = \frac{\sum_j \sum_i P_{i,j} R_{i,j,k,s}}{\sum_j \sum_i P_{i,j}}$$

where $R_{i,j,k,s}$ is the relative dry mass ratio compared to the surface. The total mass loading and relative chemical composition are unchanged.

We analyze global and regional variations of η, as well as that for the driving factors. The definition of each region used in this study is summarized in Figure A3.

3 Results and Discussion

3.1 Global Spatial Pattern of η

The top panel of Figure 1~~Figure 1~~ shows the observationally based annual mean η, inferred from the ratio of ground-measured $PM_{2.5}$ to MAIAC AOD. Measurements are most dense in North America, Europe, and East Asia. The annual mean η varies substantially, from 7.8 μg/m^3 in Hawaii to ~~321~~ 504 μg/m^3 in ~~Central Asia~~Mongolia, with a PWM of ~~95.7~~96.1 μg/m^3 ~~and standard deviation (σ) of 36.6 μg/m^3~~. Higher PWM η of ~~132~~ 196 μg/m^3 to ~~154~~ 154 μg/m^3 exist over desert regions such as Africa and West Asia, followed by PWM η of 97 μg/m^3 to ~~121~~ 119 μg/m^3 ~~by~~ over regions strongly influenced by anthropogenic aerosols, such as East Asia and~~,~~ South Asia (Figure A4 and Table A1). Over North America, η is around 60 μg/m^3 in the east and in California, which is more than double that in the Rockies, driven by the spatial pattern of surface $PM_{2.5}$ (Figure A4). The PWM η in North America of ~~60.3~~59.8 μg/m^3 is about 30% lower than the global PWM. The η

pattern found here is similar to that reported by Jin et al. (2020) for the U.S. In Europe, η also varies noticeably between the east and the west, driven by the spatial pattern of surface $PM_{2.5}$, as $PM_{2.5}$ increases by 60% from west to east while AOD increases by only 8%. The PWM η in Europe is 9~~4.0~~ 2.3 μg/m^3, slightly lower than the global PWM. In Asia, measured η is concentrated in China and India. In China, the η spatial pattern shows a clear distinction between the northern and southern regions, driven by the higher AOD in the south (Figure A5), where relative humidity is high. A similar η spatial pattern and a negative correlation between η and RH are reported by Yang et al. (2019). In India, η is highest in the northwest, with a PWM η of ~~128~~ 129 μg/m^3, and decreases to about 80 μg/m^3 toward the east and the south. Both $PM_{2.5}$ and AOD follow the same spatial pattern, while $PM_{2.5}$ exhibits a stronger decreasing tendency (Figure A4 and Figure A5). PWM η in Asia is ~~100~~ 102 μg/m^3, the highest among the populous regions and ~~4.5~~6.0% higher than the global PWM. Globally, from west to east, η increases by about ~~62~~70%, despite that both $PM_{2.5}$ and AOD increased more than threefold (Figure A6). The coefficient of variation (standard deviation divided by mean) in η is higher in Europe (μ = 0.31) and Asia (μ = 0.~~34~~36), than North America (μ = 0.2~~5~~3, Figure A6).

The bottom panel in Figure 1~~Figure 1~~ shows the GCHP simulated η, the ratio between simulated 24-hour mean surface $PM_{2.5}$ and simulated total column AOD at satellite overpass time. The simulation generally reproduces the global observations of η with a tendency for high values in arid regions influenced by dust and low values in regions distant from strong surface sources. The simulated global ~~simulated~~ PWM η is 2~~4~~% higher than the observations (~~99.5~~98.1 μg/m^3 vs. ~~95.7~~96.1 μg/m^3), mostly driven by an overestimation in East Asia (10~~8~~7 μg/m^3 vs. ~~100~~96.9 μg/m^3), that reflects an overestimation of PWM $PM_{2.5}$ (4~~7.0~~3.3 μg/m^3 vs. ~~43.6~~38.0 μg/m^3). The simulation generally reproduces the regional spatial pattern in North America and Asia but underestimates the η variability in Europe as it overestimates η in central Europe and underestimates η in Eastern Europe, due to positive bias in simulated $PM_{2.5}$ in central Europe and positive bias in simulated AOD in Eastern Europe. Nonetheless, the PWM η in Europe (~~84.1~~83.6 μg/m^3) is within ~~11~~9.4% of observations. Globally, there is overall consistency between the simulated η and observed η, with a correlation of 0.~~64~~59, resulting in a high degree of consistency between geophysical $PM_{2.5}$ and measured $PM_{2.5}$ (r = 0.~~90~~89, Figure A6). Evaluation of the simulation of $PM_{2.5}$ chemical

composition versus ground-based measurements reveals a high degree of consistency (Figure A2) that supports their further assessment of the factors affecting η.

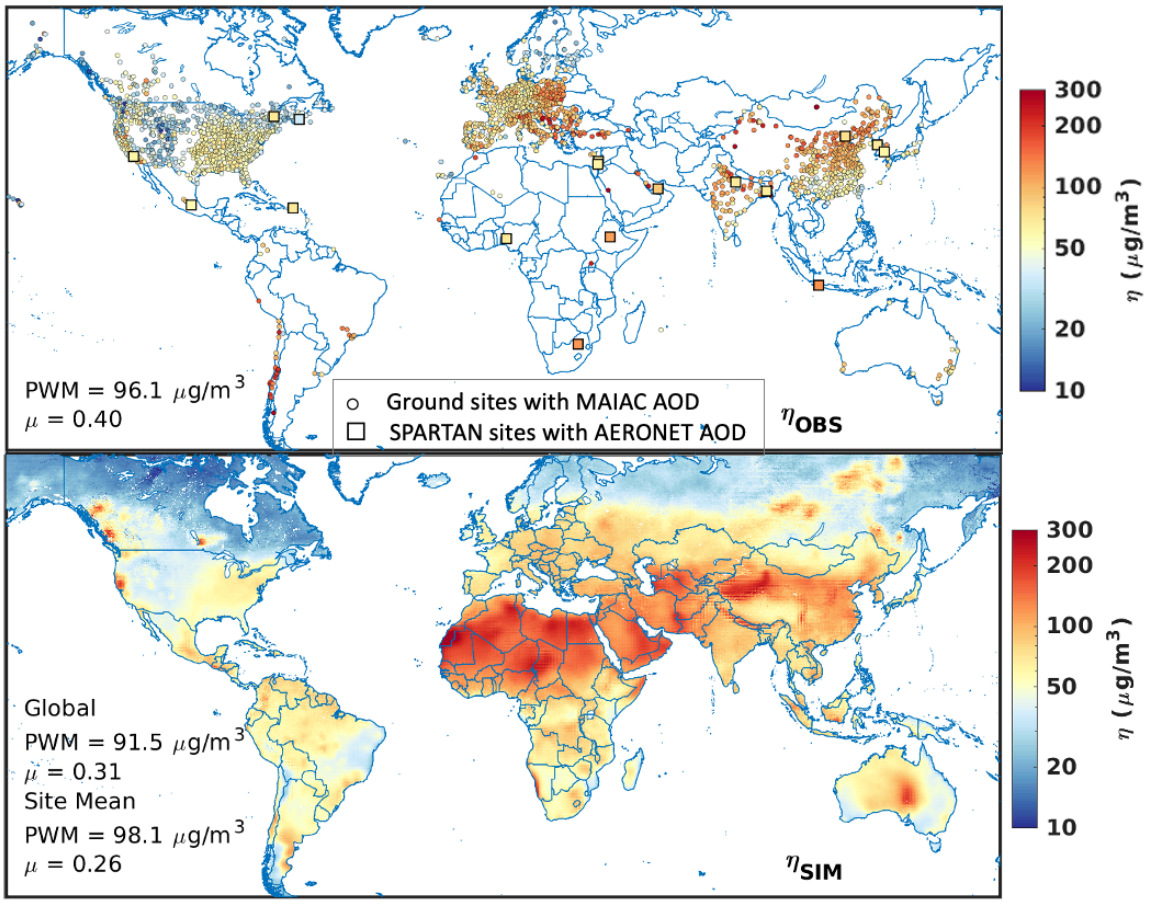
PWM = 96.1 μg/m3
μ = 0.40
Ground sites with MAIAC AOD
SPARTAN sites with AERONET AOD
ηOBS
300
200
100
50
20
10
η (μg/m3)
Global
PWM = 91.5 μg/m3
μ = 0.31
Site Mean
PWM = 98.1 μg/m3
μ = 0.26
ηSIM
300
200
100
50
20
10
η (μg/m3)

254

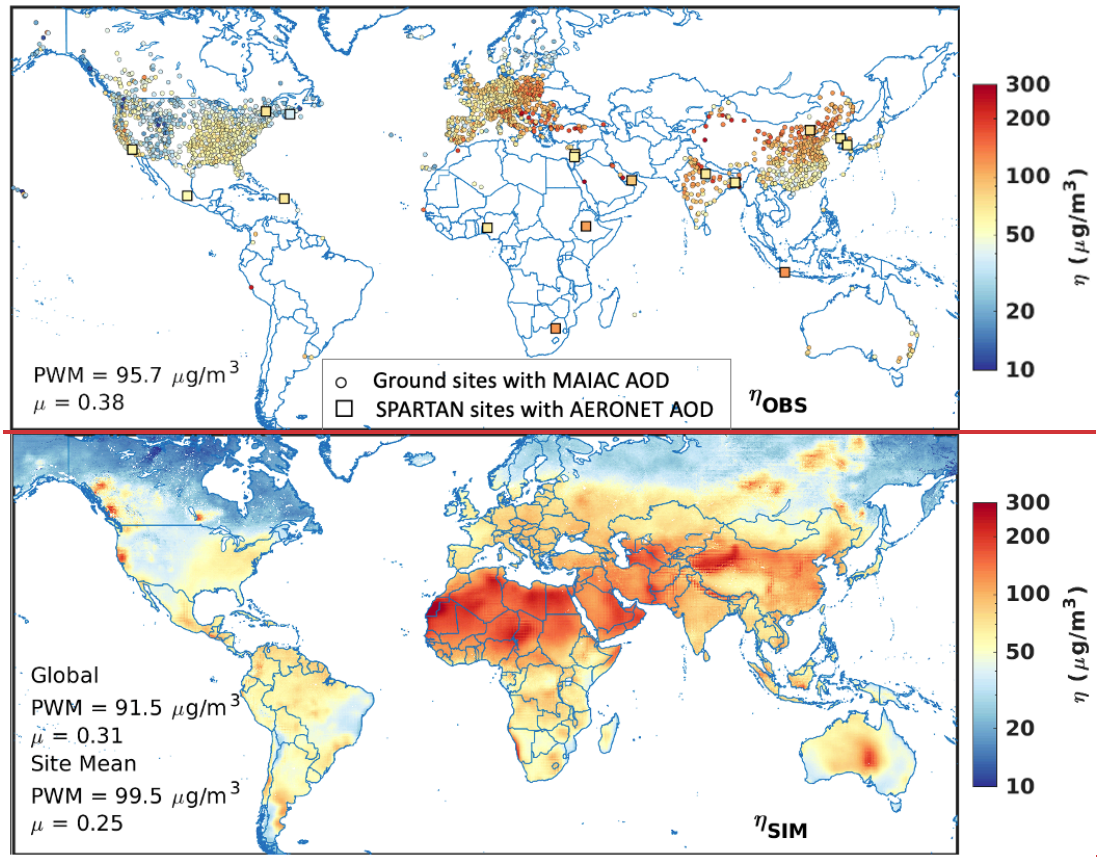

Figure 1. Observed (top) and simulated (bottom) annual mean η for 2019. Circles represent ground measurement sites from regional networks or the World Health Organization. Squares represent co-located ground measured $PM_{2.5}$ from SPARTAN and AOD from AERONET. PWM = population-weighted mean, μ = coefficient of variation (standard deviation divided by mean).

We explore the dominant driving factors for η spatial variation by calculating the spatial correlation between each candidate factor and the observation-based η. Candidate factors examined include meteorological fields (MERRA-2), aerosol vertical profile, and aerosol composition as collected from the GCHP simulation or SPARTAN. Meteorological fields include those commonly considered to represent the temporal variation in η, such as PBLH, RH at 700 hPa, wind speed at 10 m, and temperature at 2 m (Chu et al., 2015; Damascena et al., 2021; He et al., 2021; Yang et al., 2019). The aerosol vertical profile is represented as the AOD fraction below 1 km (AOD % below 1 km). Aerosol composition includes SNA, OM, dust, black carbon, and sea salt, all represented as the fractional contributions (%) to surface $PM_{2.5}$. Figure 2 shows the spatial correlation of annual mean factors versus observation-based η. Aerosol components, particularly

those with strong primary sources (dust, OM, and black carbon), exhibit the strongest correlations (>0.~~3~~27) with observationally based η. Significant positive correlations are found for mineral dust and black carbon, both of which are non- or weakly-hygroscopic. Significant negative correlations are found for organic matter and sea salt, reflecting a weak connection between surface concentrations and AOD aloft. Processes are further discussed in sections 3.2 and 3.4. The aerosol vertical profile exhibits a moderate correlation with η (0.~~18~~14), which is notably higher than any meteorological factors (~~<0.12~~≤0.10). Ground-based data from SPARTAN and AERONET corroborate the correlation between aerosol composition and η (Figure A7). We thus focus further analysis in Sections 3.2-3.4 on the two main drivers in η: aerosol composition and aerosol vertical profile.

The ~~indicators~~ drivers of spatial variation in η found here differ from that for temporal variation of η in prior work (e.g. He et al. 2021), reflecting the different processes involved. Meteorological parameters drive short-term variability in the aerosol vertical profile, such as day-to-day variation in mixed layer depth or in advection from a point source. In contrast, the spatial variation in annual mean η reflects the spatial variation in processes affecting the long-term relation of surface $PM_{2.5}$ at controlled RH of 35% with AOD at ambient RH. Aerosol composition and the aerosol vertical profile reflect spatial variation in aerosol hygroscopicity, mass extinction efficiency, and sources. The following sections explore how aerosol composition and aerosol vertical profile vary globally and examine how they affect the spatial pattern of η by conducting two sensitivity tests. In each sensitivity test, we replace the spatial variability of a factor with a globally uniform value. The variability of aerosol composition and aerosol vertical profile are discussed in sections 3.2 and 3.3, respectively. The sensitivity test results are discussed in section 3.4.

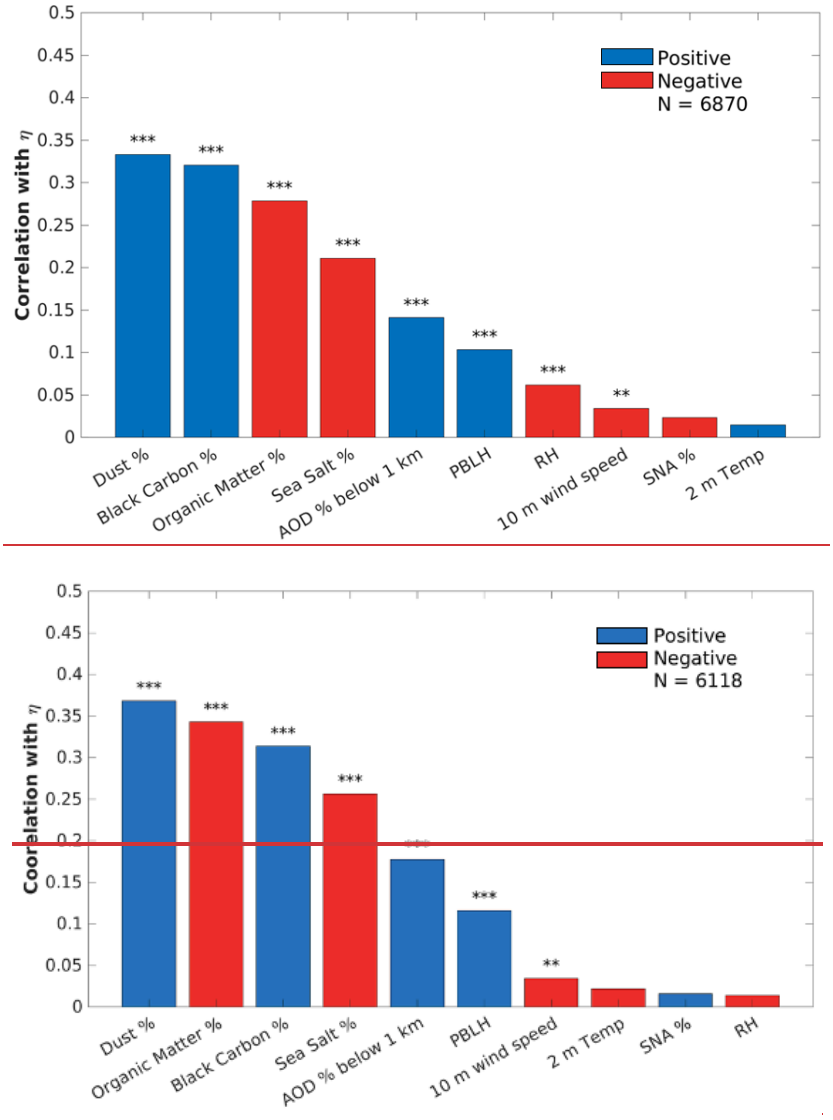

Figure 2. Spatial correlation between annual mean modeled parameters and observationally-based η. Blue bars indicate positive correlations. Red bars indicate negative correlations. Stars above each bar indicate the p-value associated with each correlation. '***' indicates the p-value is lower than 0.001 and '**' indicates lower than 0.01.

3.2 Spatial Variability in Aerosol Composition

Figure 3~~Figure 3~~ shows the simulated PWM aerosol composition globally and regionally, as well as the global area-weighted mean (AWM). The top panel shows the compositional contribution to $PM_{2.5}$. Globally, dust is the leading PWM $PM_{2.5}$ component (34.7%), followed by OM (31.9%) and SNA (29.3%). The bottom panel shows the compositional contribution to AOD. PWM AOD

composition is more evenly distributed, with more contribution from SNA (49.9%), followed by OM (27.2%) and dust (16.1%). Overall, more hygroscopic aerosols such as SNA tend to contribute a larger fraction of AOD which is at ambient RH, while less hygroscopic aerosols, such as mineral dust tend to contribute a larger fraction of $PM_{2.5}$ which is at controlled RH of 35%. The AWM $PM_{2.5}$ and AOD composition exhibit weaker contributions from SNA, primarily reflecting a larger contribution from dust in remote regions than in more densely populated areas. Over populous regions such as North America, Europe, and Southeast Asia, there are greater SNA and OM fractions than the global mean (Figure 3~~Figure 3~~). Arid regions, such as West Asia, the Middle East, North Africa, and Sub-Saharan Africa, have large fractions of non-hygroscopic mineral dust that (1) reduce aerosol mass extinction efficiency, yielding less AOD per unit mass, and (2) are unaffected by the controlled RH of $PM_{2.5}$. Both of these factors increase η in dusty regions compared with regions dominated by hygroscopic SNA aerosols.

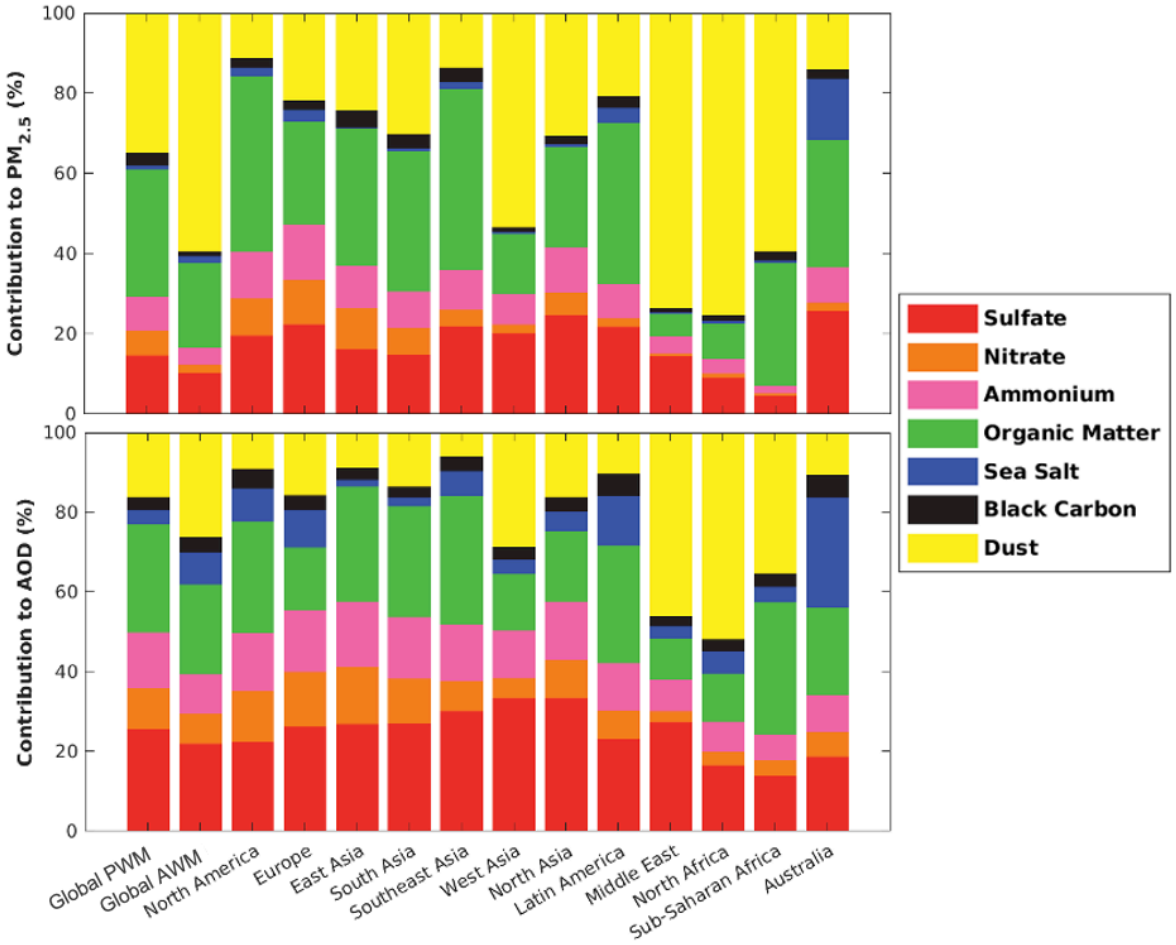

Figure 3. Global and regional PWM contributions of aerosol composition to surface $PM_{2.5}$ (top) and AOD (bottom). The global area-weighted mean (AWM) over land is also included as the second column.

3.3 Spatial Variability in Aerosol Vertical Profile

Figure 4 shows the AOD fraction below 1 km in the GEOS-Chem simulation. Globally, 35.3% of the PWM AOD is below 1 km. The PWM value is greater than the AWM value since populated areas tend to have more surface emissions of particles and precursors. Over North America, Europe, and East Asia, the PWM surface AOD fractions are much higher than the medians and AWM, indicating high spatial heterogeneity between urban and remote areas. Europe exhibits the highest variation and the largest discrepancy between PWM and AWM, reflecting the largest spatial heterogeneity in aerosol vertical profile, driven by influences from regional pollution, marine aerosols, and transported dust (Zhao et al., 2018). Southeast Asia has the highest surface AOD fraction and a large variation. Local sources, long-range transported dust, and the influence of trade winds all contribute to the unique spatial variation in aerosol vertical profile in this region (Banerjee et al., 2021; Nguyen et al., 2019). Globally, PWM values exhibit less variation than AWM, indicating moderate variation in aerosol profile across populous areas.

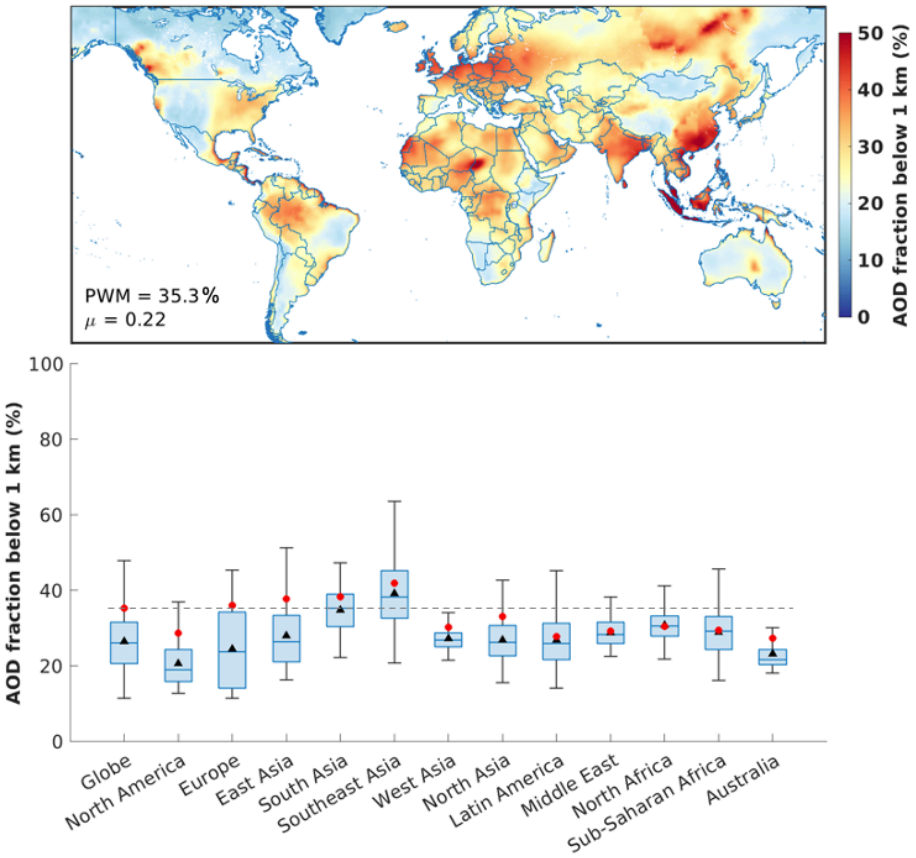

Figure 4. (Top) Map of AOD fraction below 1 km. (Bottom) Global and regional statistics for AOD fraction below 1 km. Black triangles show the area-weighted mean. Red circles show the PWM. The line inside each box is the sample median. Each box's top and bottom edges are the 75 and 25 quartiles, respectively. Vertical bars are the maximum and minimum values within 1.5 times the interquartile range. The dashed line indicates global PWM.

3.4 Sensitivity Tests with Globally Uniform Parameters

Figure 5~~Figure 5~~ shows the global changes in the spatial variation in η due to variations in aerosol chemical composition (top) and aerosol vertical profile (bottom), the two main drivers found in Figure 2. Globally, neglect of spatial variation in aerosol composition induces a 12.3 μg/m^3 PWMD in η spatial variation. Both $PM_{2.5}$ and AOD are strongly affected by aerosol composition, following a similar spatial pattern (Figure A8). Over mid- and low-latitude areas, the change in AOD is stronger than in $PM_{2.5}$, since AOD at ambient RH is more sensitive to hygroscopicity changes. ~~which gives~~This yields the opposite pattern in the η. Neglect of spatial variation in chemical composition reduces η over North Africa and the Middle East, desert regions where

aerosols contain more weakly hygroscopic components such as mineral dust, compared to populous areas, which contain more secondary inorganic aerosol (Figure 3~~Figure 3~~). For smaller deserts in the Southwest U.S., Argentina, and Southwest Africa, the dust fractions of surface aerosols are higher than the global mean (36%, 76%, and 49%, respectively), but the dust fraction for AOD is similar to the global mean (15%, 25%, and 14%, respectively). Therefore, neglect of the spatial variation of chemical composition increases η over these small deserts by increasing the fraction of hygroscopic components in $PM_{2.5}$ and leaving AOD almost unchanged (Figure A8). ~~It~~ Neglect of spatial variation in chemical composition also reduces η over the boreal forests~~, and the Amazon,~~ where surface aerosols ~~contain little dust and~~ are more hygroscopic compared to populous areas and show strong changes, while less so for column aerosol (Figure A8). ~~(Figure 3).~~ Neglect of spatial variation in chemical composition increases η over the eastern U.S. and eastern China, where $PM_{2.5}$ contains more hygroscopic SNA and less dust than the global mean. It also increases η in coastal regions where aerosol contains more hygroscopic sea salt than the global mean.

Neglect of spatial variation in the aerosol vertical profile induces an 8.4 $\mu g/m^3$ PWMD in η spatial variation (Figure 5~~Figure 5~~), following the spatial pattern of the change in surface $PM_{2.5}$ (Figure A9). The most apparent feature is an increase in η throughout the remote northern hemisphere, driven by an increased aerosol fraction near the surface where the fraction is normally small (Figure 4). The uniform aerosol vertical profile decreases η over northern Africa and biomass burning regions of the boreal forests, the Amazon, and Indonesia, driven by a decreased aerosol fraction near the surface in regions where that fraction is normally high.

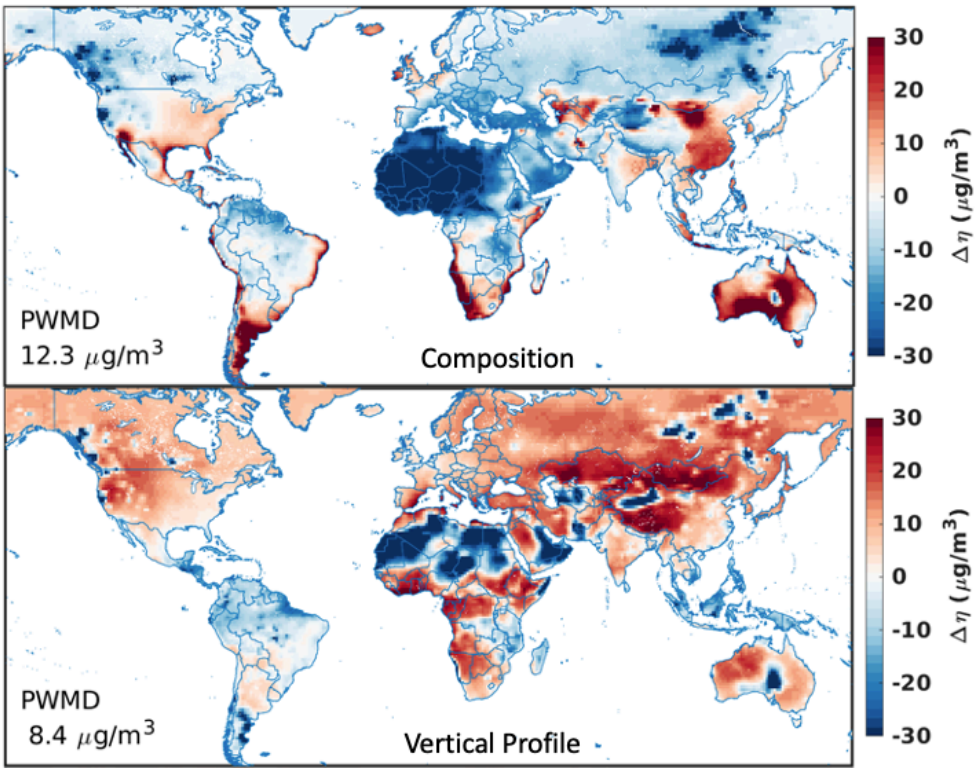

Figure 5. Changes in η (test -base) for each sensitivity test. In the first test, a global PWM aerosol composition replaces the actual composition (top). In the second test, a global PWM aerosol profile replaces the actual profiles (bottom). Numbers inset indicate population-weighted mean difference (PWMD).

Conclusion

Understanding the global variation of the $PM_{2.5}$ and AOD relationship (η) offers insight into the geophysical inference of $PM_{2.5}$ from satellite AOD observations. We collected ground-based $PM_{2.5}$ measurements from ~~6188~~ 6,870 sites and MODIS MAIAC satellite AOD throughout the year 2019 to obtain, for the first time, a global scale observationally based η map. Observed annual mean η ranges from 7.8 μg/m^3 in Hawaii to ~~321~~ 504 μg/m^3 in ~~Central Asia~~Mongolia. We observed enhanced η of ~~132~~ 196 μg/m^3 to 154 μg/m^3 over arid regions such as Africa and West Asia, due to their low aerosol extinction efficiency. Moderate η of 97 μg/m^3 to ~~121~~ 119 μg/m^3 was found in industrial areas such as East Asia and South Asia, where anthropogen~~et~~ic emissions increase the near-surface $PM_{2.5}$ concentrations. Over remote areas, low η (< 50 μg/m^3) was usually observed.

We simulated the global annual mean η with the GEOS-Chem chemical transport model in its high performance configuration (GCHP). The simulation generally represented observed η with PWM within 34% (~~99.5~~98.1 μg/m^3 vs ~~95.7~~96.1 μg/m^3) and~~,~~ a correlation of 0.59~~64~~ over the 6,~~118~~ 780 measurement sites~~, and a slope of 0.81~~. We examined the correlation between simulation and measurements to identify the two most impactful drivers for η spatial variation - aerosol composition and aerosol vertical profile, both of which strongly affect the annual mean relation of columnar AOD at ambient RH with surface $PM_{2.5}$ at controlled RH of 35%. ~~-~~We subsequently conducted sensitivity tests by eliminating the spatial variation of each of the two drivers and quantified the impact on η spatial variability. Imposing a globally uniform aerosol composition led to ~~more~~ pronounced changes (PWMD = 12.3 μg/m^3), reflecting how changes in aerosol composition affect both AOD and surface $PM_{2.5}$, due to the effects of aerosol hygroscopicity on both quantities. Imposing a globally uniform aerosol vertical profile had a moderate effect (PWMD = 8.4 μg/m^3), reflecting changes in the fraction of aerosol near the surface.

These findings motivate additional efforts to develop the simulation of aerosol composition and aerosol vertical profile. Promising avenues include: (1) enhancing global long-term measurements of $PM_{2.5}$ chemical composition to evaluate and improve simulations, (2) exploiting new and emerging information about aerosol type from satellite remote sensing (e.g. PACE, MAIA), (3) advancing simulations at finer spatial resolution to better represent processes affecting aerosol composition and vertical profile, (4) leveraging aircraft, lidar, and collected AOD-to-$PM_{2.5}$ measurements for constraints on the vertical profile, and (5) exploiting nascent capabilities in applying satellite remote sensing (e.g. TROPOMI, TEMPO, GEMS) for top-down constraints on emissions that affect aerosol composition.

Appendix

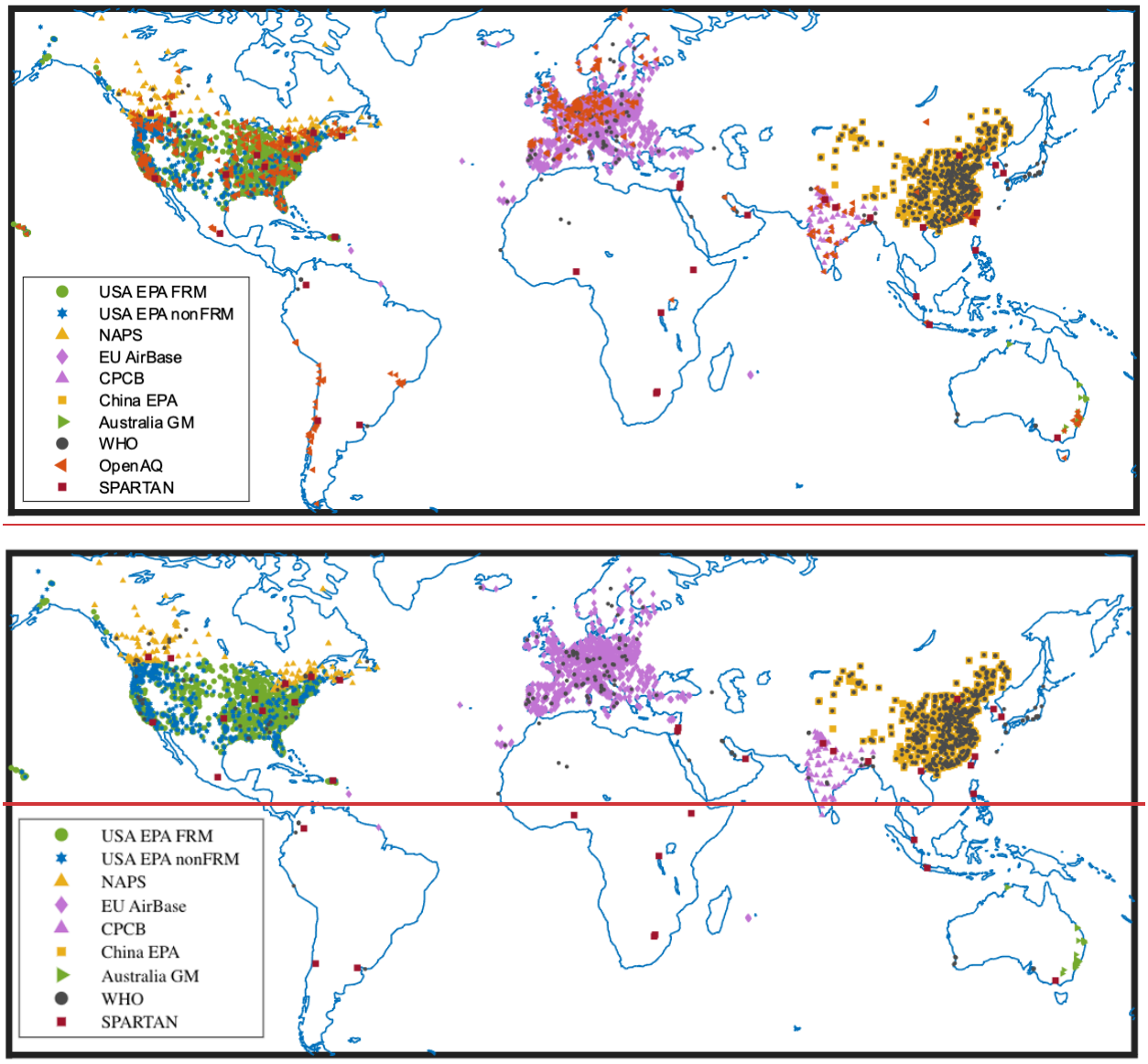

Figure A1. $PM_{2.5}$ measurement sites from publicly available networks.

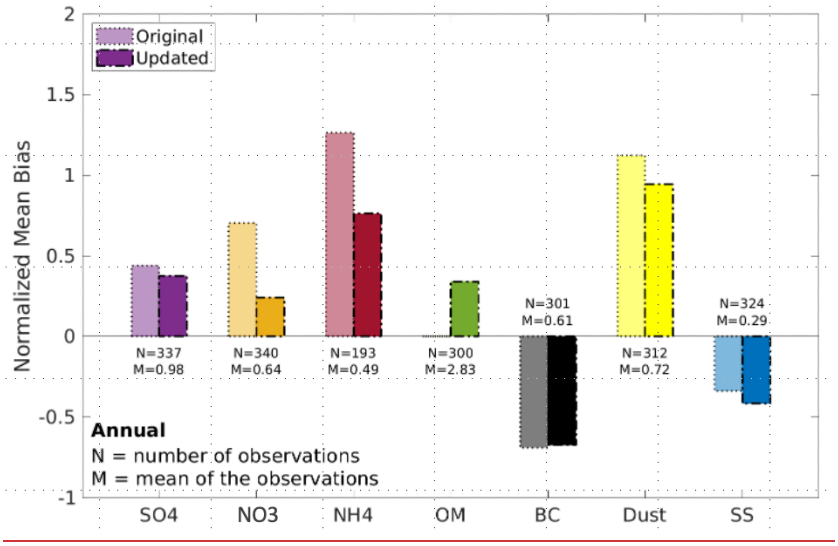

Figure A2. Normalized mean bias (NMB) between simulated $PM_{2.5}$ chemical composition and ground measurements from CSN, IMPROVE, EBAS, and SPARTAN. The original simulation is the out-of-box version of GCHP v13.4.0, the updated simulation includes adjustments such as GFED4.1s emission at daily scale, diel variation and vertical distribution of anthropogenic emissions, and 50% reduction in nitrate concentration.

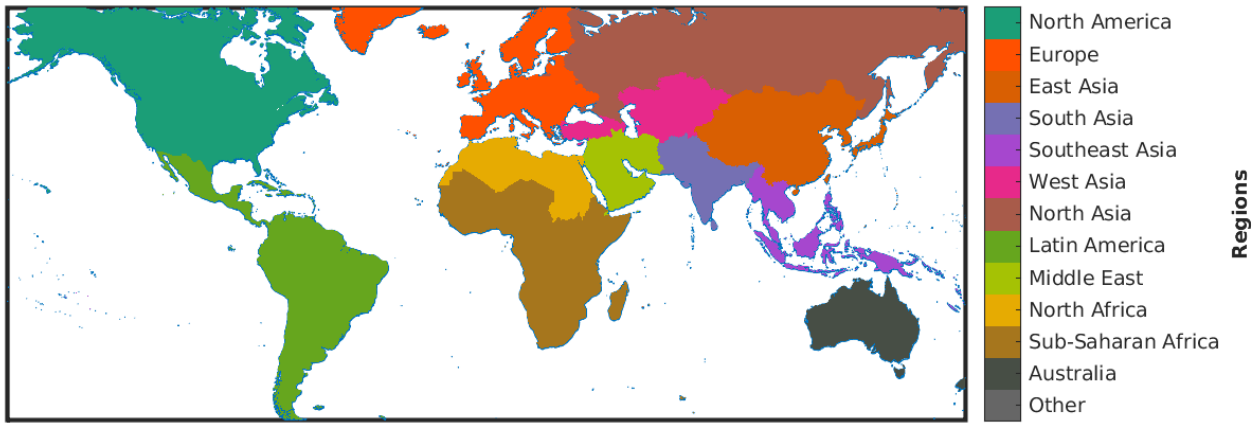

Figure A3. Region definition.

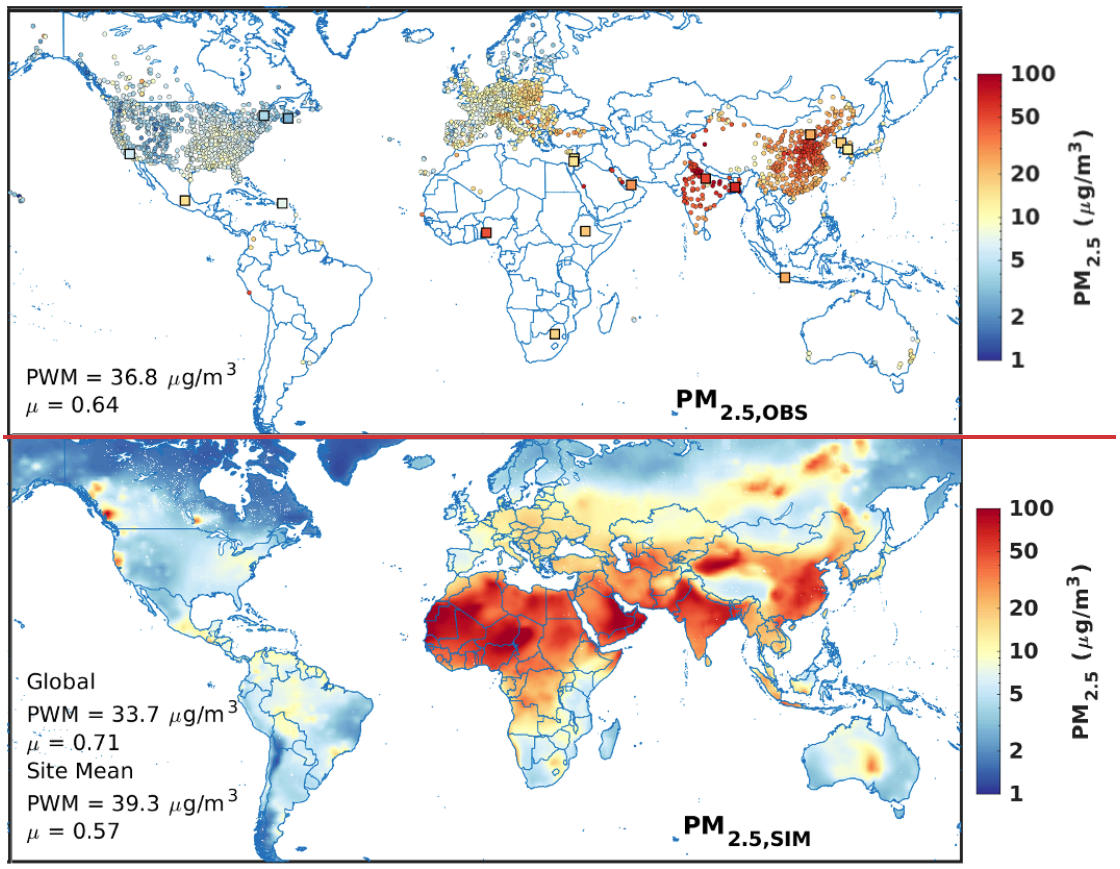
PWM = 36.8 μg/m3
μ = 0.64
PM2.5,OBS
100
50
20
10
5
2
1
PM2.5 (μg/m3)
Global
PWM = 33.7 μg/m3
μ = 0.71
Site Mean
PWM = 39.3 μg/m3
μ = 0.57
PM2.5,SIM
100
50
20
10
5
2
1
PM2.5 (μg/m3)

418

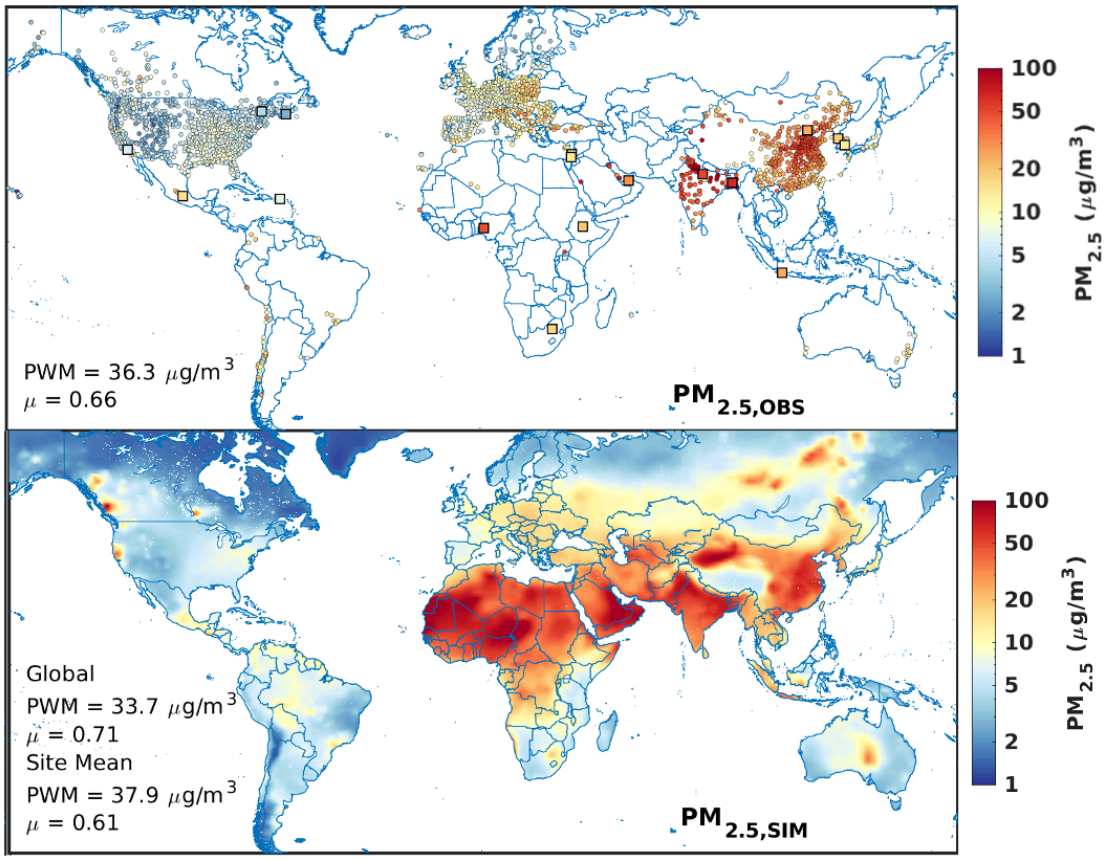

419

420 Figure A4. Observed (top) and simulated (bottom) annual mean $PM_{2.5}$ for 2019. Circles represent
421 measurement sites from regional networks or reported by the WHO. Squares represent measured $PM_{2.5}$
422 from SPARTAN. PWM = population-weighted mean, μ = coefficient of variation.

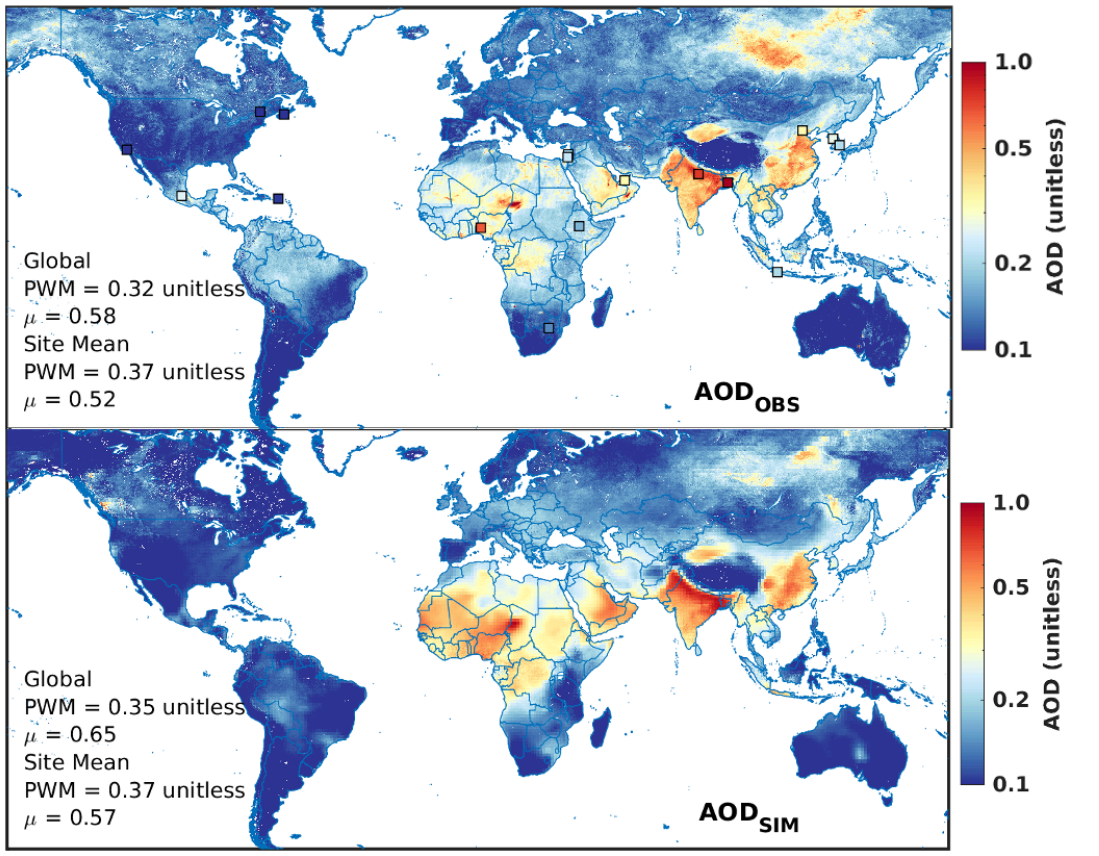
Global
PWM = 0.32 unitless
μ = 0.58
Site Mean
PWM = 0.37 unitless
μ = 0.52
AOD$_{OBS}$
1.0
0.5
0.2
0.1
AOD (unitless)
Global
PWM = 0.35 unitless
μ = 0.65
Site Mean
PWM = 0.37 unitless
μ = 0.57
AOD$_{SIM}$
1.0
0.5
0.2
0.1
AOD (unitless)

423

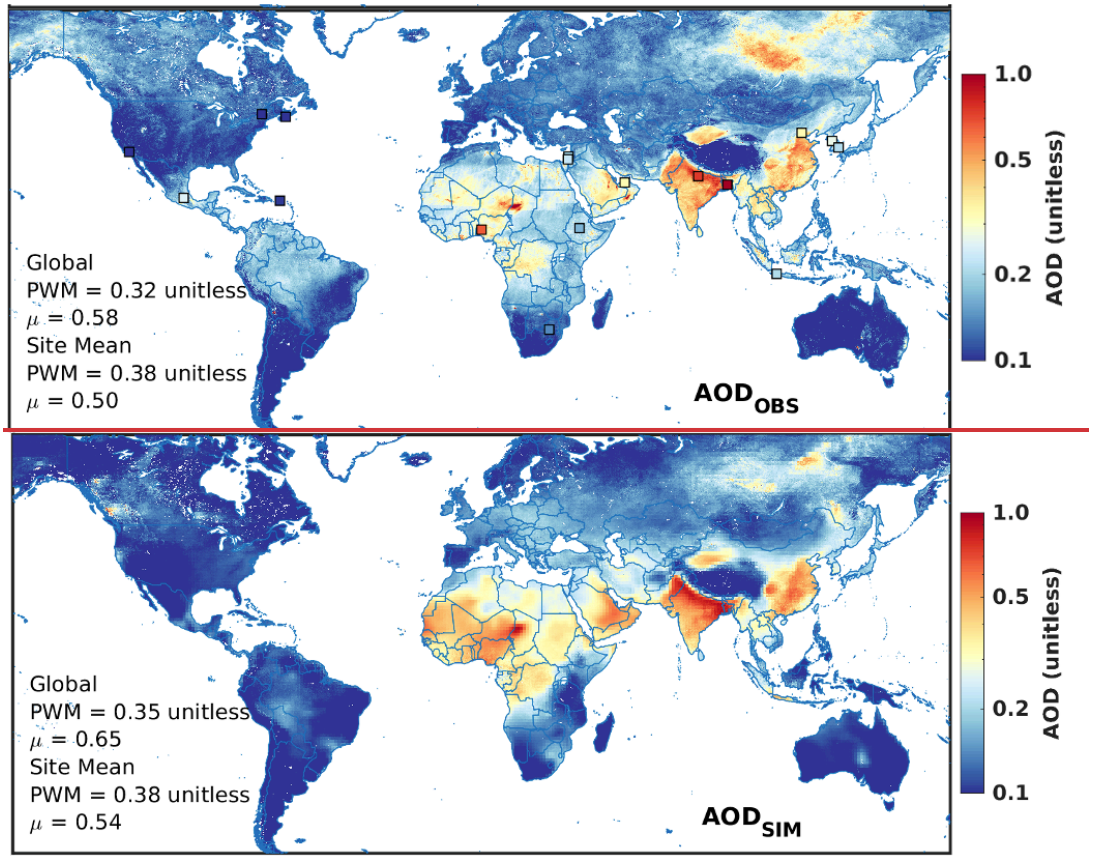

Figure A5. Satellite retrieved (top) and GCHP simulated (bottom) annual mean AOD for 2019. Squares represent ground-measured AOD from AERONET. PWM = population-weighted mean, μ = coefficient of variation.

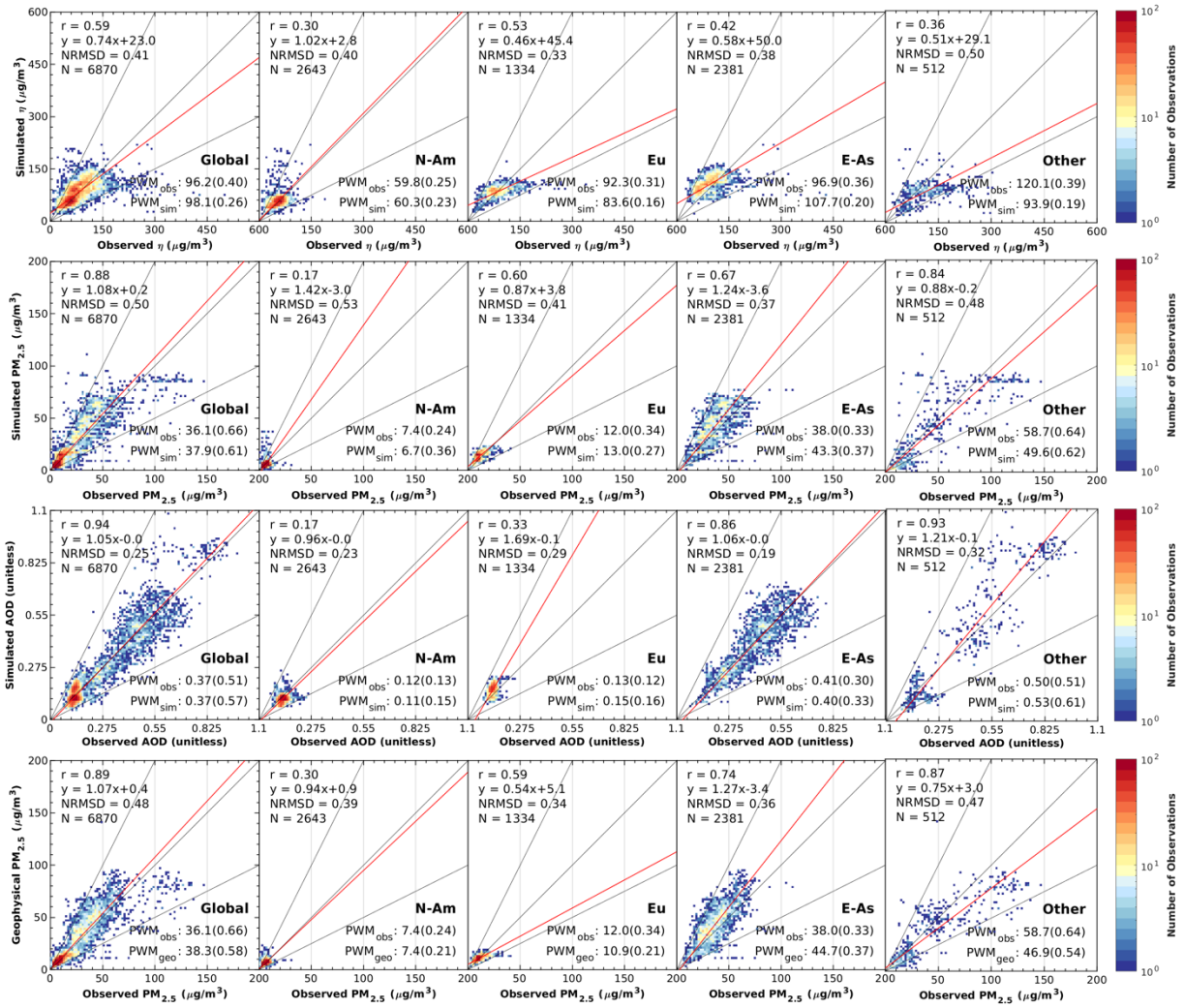
r = 0.59
y = 0.74x+23.0
NRMSD = 0.41
N = 6870
Global
PWM obs: 96.2(0.40)
PWM sim: 98.1(0.26)
r = 0.30
y = 1.02x+2.8
NRMSD = 0.40
N = 2643
N-Am
PWM obs: 59.8(0.25)
PWM sim: 60.3(0.23)
r = 0.53
y = 0.46x+45.4
NRMSD = 0.33
N = 1334
Eu
PWM obs: 92.3(0.31)
PWM sim: 83.6(0.16)
r = 0.42
y = 0.58x+50.0
NRMSD = 0.38
N = 2381
E-As
PWM obs: 96.9(0.36)
PWM sim: 107.7(0.20)
r = 0.36
y = 0.51x+29.1
NRMSD = 0.50
N = 512
Other
PWM obs: 120.1(0.39)
PWM sim: 93.9(0.19)
Simulated η (μg/m3)
Observed η (μg/m3)
r = 0.88
y = 1.08x+0.2
NRMSD = 0.50
N = 6870
Global
PWM obs: 36.1(0.66)
PWM sim: 37.9(0.61)
r = 0.17
y = 1.42x-3.0
NRMSD = 0.53
N = 2643
N-Am
PWM obs: 7.4(0.24)
PWM sim: 6.7(0.36)
r = 0.60
y = 0.87x+3.8
NRMSD = 0.41
N = 1334
Eu
PWM obs: 12.0(0.34)
PWM sim: 13.0(0.27)
r = 0.67
y = 1.24x-3.6
NRMSD = 0.37
N = 2381
E-As
PWM obs: 38.0(0.33)
PWM sim: 43.3(0.37)
r = 0.84
y = 0.88x-0.2
NRMSD = 0.48
N = 512
Other
PWM obs: 58.7(0.64)
PWM sim: 49.6(0.62)
Simulated PM2.5 (μg/m3)
Observed PM2.5 (μg/m3)
r = 0.94
y = 1.05x-0.0
NRMSD = 0.25
N = 6870
Global
PWM obs: 0.37(0.51)
PWM sim: 0.37(0.57)
r = 0.17
y = 0.96x-0.0
NRMSD = 0.23
N = 2643
N-Am
PWM obs: 0.12(0.13)
PWM sim: 0.11(0.15)
r = 0.33
y = 1.69x-0.1
NRMSD = 0.29
N = 1334
Eu
PWM obs: 0.13(0.12)
PWM sim: 0.15(0.16)
r = 0.86
y = 1.06x-0.0
NRMSD = 0.19
N = 2381
E-As
PWM obs: 0.41(0.30)
PWM sim: 0.40(0.33)
r = 0.93
y = 1.21x-0.1
NRMSD = 0.32
N = 512
Other
PWM obs: 0.50(0.51)
PWM sim: 0.53(0.61)
Simulated AOD (unitless)
Observed AOD (unitless)
r = 0.89
y = 1.07x+0.4
NRMSD = 0.48
N = 6870
Global
PWM obs: 36.1(0.66)
PWM geo: 38.3(0.58)
r = 0.30
y = 0.94x+0.9
NRMSD = 0.39
N = 2643
N-Am
PWM obs: 7.4(0.24)
PWM geo: 7.4(0.21)
r = 0.59
y = 0.54x+5.1
NRMSD = 0.34
N = 1334
Eu
PWM obs: 12.0(0.34)
PWM geo: 10.9(0.21)
r = 0.74
y = 1.27x-3.4
NRMSD = 0.36
N = 2381
E-As
PWM obs: 38.0(0.33)
PWM geo: 44.7(0.37)
r = 0.87
y = 0.75x+3.0
NRMSD = 0.47
N = 512
Other
PWM obs: 58.7(0.64)
PWM geo: 46.9(0.54)
Geophysical PM2.5 (μg/m3)
Observed PM2.5 (μg/m3)
Number of Observations

429

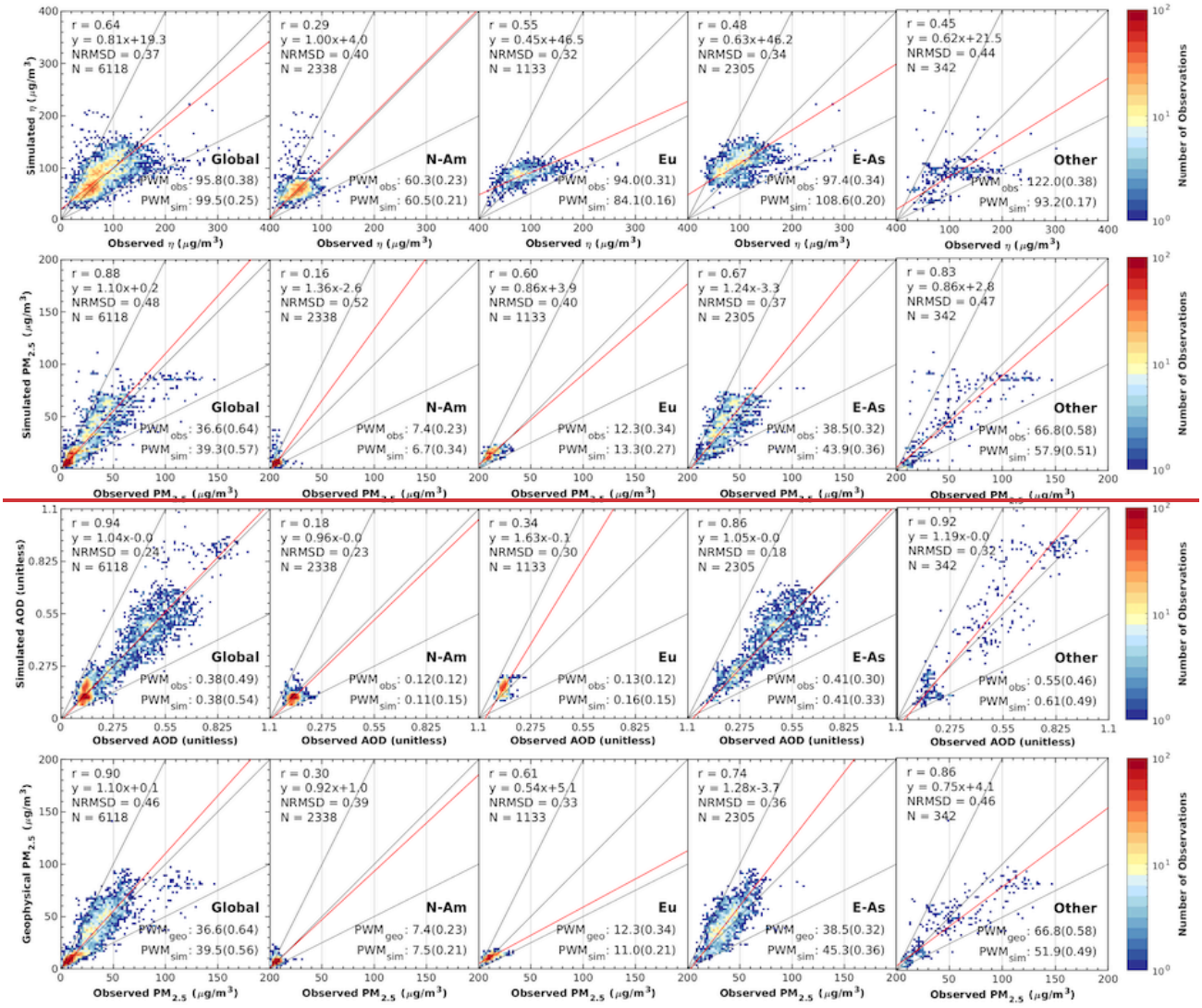

Figure A6. Scatter plots of simulated and observed η (top row), simulated and ground measured $PM_{2.5}$ (second row), simulated and MAIAC AOD (third row), and geophysical and observed $PM_{2.5}$ (bottom row). The red line shows the line of best fit using Reduced Major Axis Linear Regression. Insets on the top left show the coefficient of determination (R^2), line of best fit, normalized root mean square deviation (NRMSD), and total number of data points (N). The bottom right insets show the population-weighted mean of observed, simulated, or geophysical estimation of each dataset, coefficients of variation are bracketed. Detailed regional mean and coefficients of variation for other regions can be found in Table A1.

Table A1. Regional population-weighted mean η, $PM_{2.5}$, and AOD from both observation and simulations. Geophysical $PM_{2.5}$ is also included. Coefficients of variation are bracketed. Regional mean and coefficients of variation for North America, Europe, and East Asia can be found in Figure A6.

Region		South Asia	Southeast Asia	West Asia	Latin America	Middle East	North Africa	Sub-Saharan Africa	Australia
Number of sites		16222 0	35	43	2	46142	2932	3	56
η [μg/m^3]	Observed	121.61 19.5 (0.367)	128111.4 .6 (0.2112)	154.0 (0.23)	72.0 (0.29)	94.111 7.5 (0.516)	135.0 2.3 (0.325)	196.0 (0.01)	133.9187 .8 (0.34)
	Simulated	95.03. 4 (0.140)	82.493.8 (0.1809)	93.4 (0.03)	74.1 (0.04)	83.686. 6 (0.1821)	126.6 135.8 (0.197)	105.9 (0.01)	187.3128 .4 (0.5426)
$PM_{2.5}$ [μg/m^3]	Observed	81.075 .7 (0.451)	35.740.6 (0.4426)	22.0 (0.21)	12.0 (0.23)	21.720. 4 (0.3651)	28.732 .2 (0.5361)	24.0 (0.00)	35.546.3 (0.29)
	Simulated	70.264 .9 (0.370)	31.838.1 (0.230)	20.8 (0.08)	20.9 (0.06)	10.12 (0.3025)	38.347 .2 (0.5253)	16.7 (0.03)	90.056.6 (0.3187)
	Geo-physical	62.759 .9 (0.310)	22.736.1 (0.4329)	13.9 (0.08)	12.4 (0.08)	20.417. 6 (0.397)	27.33 3.0 (0.4049)	12.9 (0.03)	58.137.0 (0.9974)
AOD [unitless]	Observed	0.637 (0.295)	0.27 38 (0.305)	0.14 (0.08)	0.17 (0.03)	0.204 (0.3221)	0.231 (0.3028)	0.12 (0.01)	0.2730 (0.5266)
	Simulated	0.6973 (0.3628)	0.4038 (0.128)	0.22 (0.09)	0.28 (0.02)	0.2112 (0.2314)	0.29 33 (0.342)	0.16 (0.01)	0.3751 (0.4726)

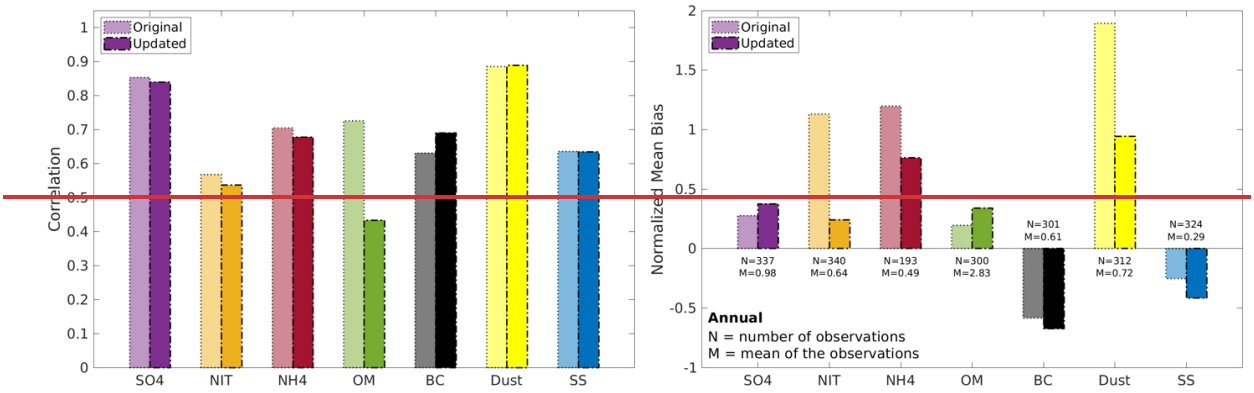

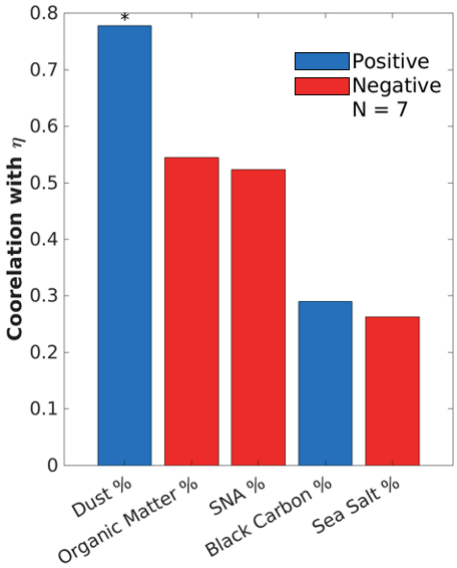

Figure A7. Correlation with η of ground-measured aerosol fractional composition from SPARTAN. Organic matter is inferred through residual (Snider et al., 2016). Blue bars indicate positive correlations. Red bars indicate negative correlations. Stars above each bar indicate the p-value associated with each correlation. '***' means the p-value is lower than 0.001, '**' means lower than 0.01, and '*' means lower than 0.5.

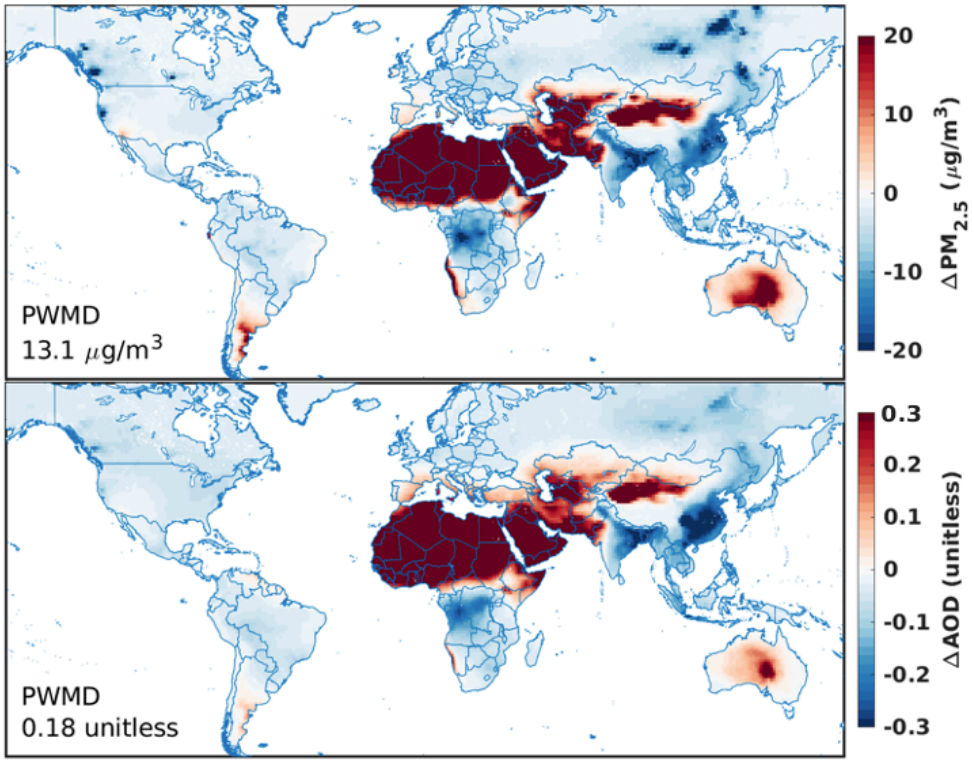

451

452 Figure A8. Changes in $PM_{2.5}$ (top) and AOD (bottom) (test - base) when imposing a global PWM aerosol
453 composition.

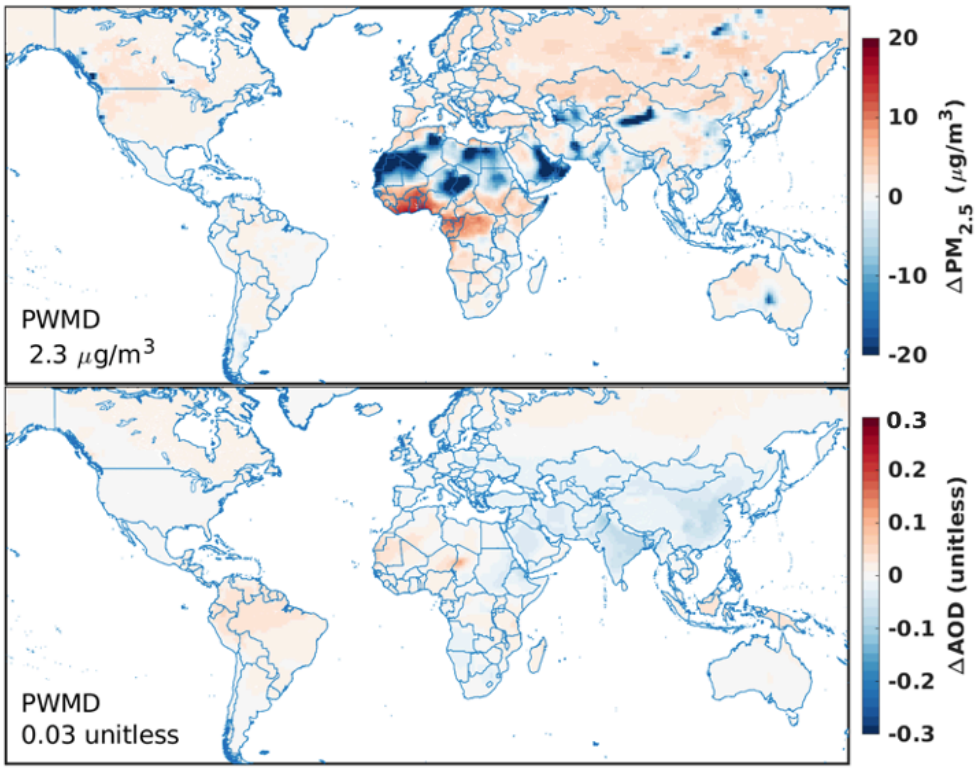

454

455 Figure A9. Changes in $PM_{2.5}$ (top) and AOD (bottom) (test - base) when imposing a global PWM aerosol
456 profile.

457 *Data availability.* GEOS-Chem in its high-performance configuration version 13.4.0 can be
458 downloaded at https://zenodo.org/records/6564711.

459 *Author contributions.* HZ and RVM designed the study. HZ performed the data analysis and model
460 simulation with contributions from AvD, CL, YL, DZ, JM, MH & IS. AvD contributed to the
461 compiled the MAIAC AOD dataset and ground-based observation datasets for $PM_{2.5}$. AL
462 contributed to the original MAIAC AOD dataset. CRO and XL contributed to the SPARTAN data
463 utilization and analysis. The manuscript was written by HZ and RVM with contributions from all
464 authors.

465 *Competing interests.* The authors declare no competing financial interest.

466 *Acknowledgment.* This work was supported by NASA Grant 80NSSC22K0200. We thank Dr. Mi
467 Zhou from Princeton University for providing ground based $PM_{2.5}$ data over India.

468

Reference

Amos, H. M., Jacob, D. J., Holmes, C. D., Fisher, J. A., Wang, Q., Yantosca, R. M., Corbitt, E. S., Galarneau, E., Rutter, A. P., Gustin, M. S., Steffen, A., Schauer, J. J., Graydon, J. A., St Louis, V. L., Talbot, R. W., Edgerton, E. S., Zhang, Y., and Sunderland, E. M.: Gas-particle partitioning of atmospheric Hg(II) and its effect on global mercury deposition, Atmospheric Chemistry and Physics, 12, 591–603, https://doi.org/10.5194/acp-12-591-2012, 2012.

Banerjee, T., Shitole, A. S., Mhawish, A., Anand, A., Ranjan, R., Khan, M. F., Srithawirat, T., Latif, M. T., and Mall, R. K.: Aerosol Climatology Over South and Southeast Asia: Aerosol Types, Vertical Profile, and Source Fields, Journal of Geophysical Research: Atmospheres, 126, e2020JD033554, https://doi.org/10.1029/2020JD033554, 2021.

Benavente, N. R., Vara-Vela, A. L., Nascimento, J. P., Acuna, J. R., Damascena, A. S., de Fatima Andrade, M., and Yamasoe, M. A.: Air quality simulation with WRF-Chem over southeastern Brazil, part I: Model description and evaluation using ground-based and satellite data, Urban Climate, 52, 101703, https://doi.org/10.1016/j.uclim.2023.101703, 2023.

Bieser, J., Aulinger, A., Matthias, V., Quante, M., and Denier Van Der Gon, H. A. C.: Vertical emission profiles for Europe based on plume rise calculations, Environmental Pollution, 159, 2935–2946, https://doi.org/10.1016/J.ENVPOL.2011.04.030, 2011.

Brauer, M., Roth, G. A., Aravkin, A. Y., Zheng, P., Abate, K. H., Abate, Y. H., Abbafati, C., Abbasgholizadeh, R., Abbasi, M. A., Abbasian, M., Abbasifard, M., Abbasi-Kangevari, M., ElHafeez, S. A., Abd-Elsalam, S., Abdi, P., Abdollahi, M., Abdoun, M., Abdulah, D. M., Abdullahi, A., Abebe, M., Abedi, A., Abedi, A., Abegaz, T. M., Zuñiga, R. A. A., Abiodun, O., Abiso, T. L., Aboagye, R. G., Abolhassani, H., Abouzid, M., Aboye, G. B., Abreu, L. G., Abualruz, H., Abubakar, B., Abu-Gharbieh, E., Abukhadijah, H. J. J., Aburuz, S., Abu-Zaid, A., Adane, M. M., Addo, I. Y., Addolorato, G., Adedoyin, R. A., Adekanmbi, V., Aden, B., Adetunji, J. B., Adeyeoluwa, T. E., Adha, R., Adibi, A., Adnani, Q. E. S., Adzigbli, L. A., Afolabi, A. A., Afolabi, R. F., Afshin, A., Afyouni, S., Afzal, M. S., Afzal, S., Agampodi, S. B., Agbozo, F., Aghamiri, S., Agodi, A., Agrawal, A., Agyemang-Duah, W., Ahinkorah, B. O., Ahmad, A., Ahmad, D., Ahmad, F., Ahmad, N., Ahmad, S., Ahmad, T., Ahmed, A., Ahmed, A., Ahmed, A., Ahmed, L. A., Ahmed, M. B., Ahmed, S., Ahmed, S. A., Ajami, M., Akalu, G. T., Akara, E. M., Akbarialiabad, H., Akhlaghi, S., Akinosoglou, K., Akinyemiju, T., Akkaif, M. A., Akkala, S., Akombi-Inyang, B., Awaidy, S. A., Hasan, S. M. A., Alahdab, F., AL-Ahdal, T. M. A., Alalalmeh, S. O., Alalwan, T. A., Al-Aly, Z., Alam, K., Alam, N., Alanezi, F. M., Alanzi, T. M., Albakri, A., AlBataineh, M. T., Aldhaleei, W. A., et al.: Global burden and strength of evidence for 88 risk factors in 204 countries and 811 subnational locations, 1990–2021: a systematic analysis for the Global Burden of Disease Study 2021, The Lancet, 403, 2162–2203, https://doi.org/10.1016/S0140-6736(24)00933-4, 2024.

Burnett, R., Chen, H., Szyszkowicz, M., Fann, N., Hubbell, B., Pope, C. A., Apte, J. S., Brauer, M., Cohen, A., Weichenthal, S., Coggins, J., Di, Q., Brunekreef, B., Frostad, J., Lim, S. S., Kan, H., Walker, K. D., Thurston, G. D., Hayes, R. B., Lim, C. C., Turner, M. C., Jerrett, M., Krewski, D., Gapstur, S. M., Diver, W. R., Ostro, B., Goldberg, D., Crouse, D. L., Martin, R. V., Peters, P., Pinault, L., Tjepkema, M., Van Donkelaar, A., Villeneuve, P. J., Miller, A. B., Yin, P., Zhou, M.,

Wang, L., Janssen, N. A. H., Marra, M., Atkinson, R. W., Tsang, H., Thach, T. Q., Cannon, J. B., Allen, R. T., Hart, J. E., Laden, F., Cesaroni, G., Forastiere, F., Weinmayr, G., Jaensch, A., Nagel, G., Concin, H., and Spadaro, J. V.: Global estimates of mortality associated with longterm exposure to outdoor fine particulate matter, Proceedings of the National Academy of Sciences of the United States of America, 115, 9592–9597, https://doi.org/10.1073/pnas.1803222115, 2018.

Canagaratna, M. R., Jimenez, J. L., Kroll, J. H., Chen, Q., Kessler, S. H., Massoli, P., Hildebrandt Ruiz, L., Fortner, E., Williams, L. R., Wilson, K. R., Surratt, J. D., Donahue, N. M., Jayne, J. T., and Worsnop, D. R.: Elemental ratio measurements of organic compounds using aerosol mass spectrometry: Characterization, improved calibration, and implications, Atmospheric Chemistry and Physics, 15, 253–272, https://doi.org/10.5194/acp-15-253-2015, 2015.

Center for International Earth Science Information Network - CIESIN: Gridded Population of the World, Version 4 (GPWv4): Population Density, Revision 11, 2018.

Christidis, T., Erickson, A. C., Pappin, A. J., Crouse, D. L., Pinault, L. L., Weichenthal, S. A., Brook, J. R., van Donkelaar, A., Hystad, P., Martin, R. V., Tjepkema, M., Burnett, R. T., and Brauer, M.: Low concentrations of fine particle air pollution and mortality in the Canadian Community Health Survey cohort, Environmental Health, 18, 84, https://doi.org/10.1186/s12940-019-0518-y, 2019.

Chu, D. A., Ferrare, R., Szykman, J., Lewis, J., Scarino, A., Hains, J., Burton, S., Chen, G., Tsai, T., Hostetler, C., Hair, J., Holben, B., and Crawford, J.: Regional characteristics of the relationship between columnar AOD and surface PM2.5: Application of lidar aerosol extinction profiles over Baltimore-Washington Corridor during DISCOVER-AQ, Atmospheric Environment, 101, 338e349-349, https://doi.org/10.1016/j.atmosenv.2014.11.034, 2015.

Cohen, A. J., Brauer, M., Burnett, R., Anderson, H. R., Frostad, J., Estep, K., Balakrishnan, K., Brunekreef, B., Dandona, L., Dandona, R., Feigin, V., Freedman, G., Hubbell, B., Jobling, A., Kan, H., Knibbs, L., Liu, Y., Martin, R., Morawska, L., Pope, C. A., Shin, H., Straif, K., Shaddick, G., Thomas, M., van Dingenen, R., van Donkelaar, A., Vos, T., Murray, C. J. L., and Forouzanfar, M. H.: Estimates and 25-year trends of the global burden of disease attributable to ambient air pollution: an analysis of data from the Global Burden of Diseases Study 2015, The Lancet, 389, 1907–1918, https://doi.org/10.1016/S0140-6736(17)30505-6, 2017.

Damascena, A. S., Yamasoe, M. A., Martins, V. S., Rosas, J., Benavente, N. R., Sánchez, M. P., Tanaka, N. I., and Saldiva, P. H. N.: Exploring the relationship between high-resolution aerosol optical depth values and ground-level particulate matter concentrations in the Metropolitan Area of São Paulo, Atmospheric Environment, 244, 117949, https://doi.org/10.1016/j.atmosenv.2020.117949, 2021.

Di, Q., Kloog, I., Koutrakis, P., Lyapustin, A., Wang, Y., and Schwartz, J.: Assessing PM2.5 Exposures with High Spatiotemporal Resolution across the Continental United States, Environmental Science and Technology, 50, 4712–4721, https://doi.org/10.1021/acs.est.5b06121, 2016.

van Donkelaar, A., Martin, R. V., and Park, R. J.: Estimating ground-level PM2.5 using aerosol optical depth determined from satellite remote sensing, Journal of Geophysical Research Atmospheres, 111, 1–10, https://doi.org/10.1029/2005JD006996, 2006.

van Donkelaar, A., Martin, R. V., Brauer, M., Kahn, R., Levy, R., Verduzco, C., and Villeneuve, P. J.: Global estimates of ambient fine particulate matter concentrations from satellite-based aerosol optical depth: Development and application, Environmental Health Perspectives, 118, 847–855, https://doi.org/10.1289/ehp.0901623, 2010.

van Donkelaar, A., Martin, R. V., Spurr, R. J. D., Drury, E., Remer, L. A., Levy, R. C., and Wang, J.: Optimal estimation for global ground-level fine particulate matter concentrations, Journal of Geophysical Research Atmospheres, 118, 5621–5636, https://doi.org/10.1002/jgrd.50479, 2013.

van Donkelaar, A., Martin, R. V., Spurr, R. J. D., and Burnett, R. T.: High-Resolution Satellite-Derived PM2.5 from Optimal Estimation and Geographically Weighted Regression over North America, Environmental Science and Technology, 49, 10482–10491, https://doi.org/10.1021/acs.est.5b02076, 2015.

van Donkelaar, A., Martin, R. V., Brauer, M., Hsu, N. C., Kahn, R. A., Levy, R. C., Lyapustin, A., Sayer, A. M., and Winker, D. M.: Global Estimates of Fine Particulate Matter using a Combined Geophysical-Statistical Method with Information from Satellites, Models, and Monitors, Environmental Science and Technology, 50, 3762–3772, https://doi.org/10.1021/acs.est.5b05833, 2016.

Eastham, S. D., Long, M. S., Keller, C. A., Lundgren, E., Yantosca, R. M., Zhuang, J., Li, C., Lee, C. J., Yannetti, M., Auer, B. M., Clune, T. L., Kouatchou, J., Putman, W. M., Thompson, M. A., Trayanov, A. L., Molod, A. M., Martin, R. V., and Jacob, D. J.: GEOS-Chem high performance (GCHP v11-02c): A next-generation implementation of the GEOS-Chem chemical transport model for massively parallel applications, Geoscientific Model Development, 11, 2941–2953, https://doi.org/10.5194/gmd-11-2941-2018, 2018.

Fairlie, D. T., Jacob, D. J., and Park, R. J.: The impact of transpacific transport of mineral dust in the United States, Atmospheric Environment, 41, 1251–1266, https://doi.org/10.1016/j.atmosenv.2006.09.048, 2007.

Ford, B. and Heald, C. L.: Exploring the uncertainty associated with satellite-based estimates of premature mortality due to exposure to fine particulate matter, Atmospheric Chemistry and Physics Discussions, 15, 25329–25380, https://doi.org/10.5194/acpd-15-25329-2015, 2015.

Fountoukis, C. and Nenes, A.: ISORROPIAII: A computationally efficient thermodynamic equilibrium model for K+-Ca2+-Mg2+-NH4+-Na+-SO42--NO3--Cl--H2O aerosols, Atmospheric Chemistry and Physics, 7, 4639–4659, https://doi.org/10.5194/acp-7-4639-2007, 2007.

Geng, G., Zhang, Q., Tong, D., Li, M., Zheng, Y., Wang, S., and He, K.: Chemical composition of ambient PM2. 5 over China and relationship to precursor emissions during 2005-2012, Atmospheric Chemistry and Physics, 17, 9187–9203, https://doi.org/10.5194/acp-17-9187-2017, 2017.

Giles, D. M., Sinyuk, A., Sorokin, M. G., Schafer, J. S., Smirnov, A., Slutsker, I., Eck, T. F., Holben, B. N., Lewis, J. R., Campbell, J. R., Welton, E. J., Korkin, S. V., and Lyapustin, A. I.: Advancements in the Aerosol Robotic Network (AERONET) Version 3 database - Automated near-real-time quality control algorithm with improved cloud screening for Sun photometer aerosol optical depth (AOD) measurements, Atmospheric Measurement Techniques, 12, 169–209, https://doi.org/10.5194/amt-12-169-2019, 2019.

Guo, J., Xia, F., Zhang, Y., Liu, H., Li, J., Lou, M., He, J., Yan, Y., Wang, F., Min, M., and Zhai, P.: Impact of diurnal variability and meteorological factors on the PM2.5 - AOD relationship: Implications for PM2.5 remote sensing, Environmental Pollution, 221, 94–104, https://doi.org/10.1016/j.envpol.2016.11.043, 2017.

Gupta, P., Christopher, S. A., Wang, J., Gehrig, R., Lee, Y., and Kumar, N.: Satellite remote sensing of particulate matter and air quality assessment over global cities, Atmospheric Environment, 40, 5880–5892, https://doi.org/10.1016/j.atmosenv.2006.03.016, 2006.

Hammer, M. S., Martin, R. V., Van Donkelaar, A., Buchard, V., Torres, O., Ridley, D. A., and Spurr, R. J. D.: Interpreting the ultraviolet aerosol index observed with the OMI satellite instrument to understand absorption by organic aerosols: Implications for atmospheric oxidation and direct radiative effects, Atmospheric Chemistry and Physics, 16, 2507–2523, https://doi.org/10.5194/acp-16-2507-2016, 2016.

Hao, H., Wang, Y., Zhu, Q., Zhang, H., Rosenberg, A., Schwartz, J., Amini, H., van Donkelaar, A., Martin, R., Liu, P., Weber, R., Russel, A., Yitshak-sade, M., Chang, H., and Shi, L.: National Cohort Study of Long-Term Exposure to PM2.5 Components and Mortality in Medicare American Older Adults, Environ. Sci. Technol., 57, 6835–6843, https://doi.org/10.1021/acs.est.2c07064, 2023.

He, Q., Wang, M., and Yim, S. H. L.: The spatiotemporal relationship between PM2.5 and aerosol optical depth in China: Influencing factors and implications for satellite PM2.5 estimations using MAIAC aerosol optical depth, Atmospheric Chemistry and Physics, 21, 18375–18391, https://doi.org/10.5194/acp-21-18375-2021, 2021.

Heald, C. L., Collett, J. L., Lee, T., Benedict, K. B., Schwandner, F. M., Li, Y., Clarisse, L., Hurtmans, D. R., Van Damme, M., Clerbaux, C., Coheur, P. F., Philip, S., Martin, R. V., and Pye, H. O. T.: Atmospheric ammonia and particulate inorganic nitrogen over the United States, Atmospheric Chemistry and Physics, 12, 10295–10312, https://doi.org/10.5194/acp-12-10295-2012, 2012.

Hoesly, R. M., Smith, S. J., Feng, L., Klimont, Z., Janssens-Maenhout, G., Pitkanen, T., Seibert, J. J., Vu, L., Andres, R. J., Bolt, R. M., Bond, T. C., Dawidowski, L., Kholod, N., Kurokawa, J. I., Li, M., Liu, L., Lu, Z., Moura, M. C. P., O'Rourke, P. R., and Zhang, Q.: Historical (1750-2014) anthropogenic emissions of reactive gases and aerosols from the Community Emissions Data System (CEDS), Geoscientific Model Development, 11, 369–408, https://doi.org/10.5194/gmd-11-369-2018, 2018.

Hu, X., Waller, L. A., Lyapustin, A., Wang, Y., and Liu, Y.: 10-year spatial and temporal trends of PM2.5 concentrations in the southeastern US estimated using high-resolution satellite data, Atmospheric Chemistry and Physics, 14, 6301–6314, https://doi.org/10.5194/acp-14-6301-2014, 2014.

Jaeglé, L., Quinn, P. K., Bates, T. S., Alexander, B., and Lin, J. T.: Global distribution of sea salt aerosols: New constraints from in situ and remote sensing observations, Atmospheric Chemistry and Physics, 11, 3137–3157, https://doi.org/10.5194/acp-11-3137-2011, 2011.

Jin, Q., Crippa, P., and Pryor, S. C.: Spatial characteristics and temporal evolution of the relationship between PM2.5 and aerosol optical depth over the eastern USA during 2003–2017, Atmospheric Environment, 239, 117718, https://doi.org/10.1016/j.atmosenv.2020.117718, 2020.

Jin, X., Fiore, A. M., Curci, G., Lyapustin, A., Civerolo, K., Ku, M., Van Donkelaar, A., and Martin, R. V.: Assessing uncertainties of a geophysical approach to estimate surface fine particulate matter distributions from satellite-observed aerosol optical depth, Atmospheric Chemistry and Physics, 19, 295–313, https://doi.org/10.5194/acp-19-295-2019, 2019.

Kim, P. S., Jacob, D. J., Fisher, J. A., Travis, K., Yu, K., Zhu, L., Yantosca, R. M., Sulprizio, M. P., Jimenez, J. L., Campuzano-Jost, P., Froyd, K. D., Liao, J., Hair, J. W., Fenn, M. A., Butler, C. F., Wagner, N. L., Gordon, T. D., Welti, A., Wennberg, P. O., Crounse, J. D., St. Clair, J. M., Teng, A. P., Millet, D. B., Schwarz, J. P., Markovic, M. Z., and Perring, A. E.: Sources, seasonality, and trends of southeast US aerosol: An integrated analysis of surface, aircraft, and satellite observations with the GEOS-Chem chemical transport model, Atmospheric Chemistry and Physics, 15, 10411–10433, https://doi.org/10.5194/acp-15-10411-2015, 2015.

Kondragunta, S., Veihelmann, B., and Chatfield, R. J.: Monitoring Surface PM2.5: An International Constellation Approach to Enhancing the Role of Satellite Observations, https://doi.org/10.25923/7SNZ-VN34, 2022.

Kopke, P., Hess, M., Schult, I., and Shettle, E. P.: Global Aerosol Data Set, Max-Planck-Institut Fur Meteorologie, Hamburg, https://doi.org/Report No. 243, 1997.

Latimer, R. N. C. and Martin, R. V.: Interpretation of measured aerosol mass scattering efficiency over North America using a chemical transport model, Atmospheric Chemistry and Physics, 19, 2635–2653, https://doi.org/10.5194/acp-19-2635-2019, 2019.

Li, J., Carlson, B. E., and Lacis, A. A.: How well do satellite AOD observations represent the spatial and temporal variability of PM2.5 concentration for the United States?, Atmospheric Environment, 102, 260–273, https://doi.org/10.1016/j.atmosenv.2014.12.010, 2015.

Li, Y., Martin, R. V., Li, C., Boys, B. L., van Donkelaar, A., Meng, J., and Pierce, J. R.: Development and evaluation of processes affecting simulation of diel fine particulate matter variation in the GEOS-Chem model, Atmospheric Chemistry and Physics, 23, 12525–12543, https://doi.org/10.5194/ACP-23-12525-2023, 2023.

Lin, H., Jacob, D. J., Lundgren, E. W., Sulprizio, M. P., Keller, C. A., Fritz, T. M., Eastham, S. D., Emmons, L. K., Campbell, P. C., Baker, B., Saylor, R. D., and Montuoro, R.: Harmonized Emissions Component (HEMCO) 3.0 as a versatile emissions component for atmospheric models: application in the GEOS-Chem, NASA GEOS, WRF-GC, CESM2, NOAA GEFS-Aerosol, and NOAA UFS models, Geoscientific Model Development, 14, 5487–5506, https://doi.org/10.5194/gmd-14-5487-2021, 2021.

Liu, H., Jacob, D. J., Bey, I., and Yantosca, R. M.: Constraints from 210Pb and 7Be on wet deposition and transport in a global three-dimensional chemical tracer model driven by assimilated meteorological fields, Journal of Geophysical Research Atmospheres, 106, 12109–12128, https://doi.org/10.1029/2000JD900839, 2001.

Liu, X., Turner, J. R., Hand, J. L., Schichtel, B. A., and Martin, R. V.: A Global-Scale Mineral Dust Equation, Journal of Geophysical Research: Atmospheres, 127, e2022JD036937, https://doi.org/10.1029/2022JD036937, 2022.

Liu, X., Turner, J. R., Oxford, C. R., McNeill, J., Walsh, B., Le Roy, E., Weagle, C. L., Stone, E., Zhu, H., Liu, W., Wei, Z., Hyslop, N. P., Giacomo, J., Dillner, A. M., Salam, A., Hossen, A., Islam, Z., Abboud, I., Akoshile, C., Amador-Muñoz, O., Anh, N. X., Asfaw, A., Balasubramanian, R., Chang, R. Y.-W., Coburn, C., Dey, S., Diner, D. J., Dong, J., Farrah, T., Gahungu, P., Garland, R. M., Grutter de la Mora, M., Hasheminassab, S., John, J., Kim, J., Kim, J. S., Langerman, K., Lee, P.-C., Lestari, P., Liu, Y., Mamo, T., Martins, M., Mayol-Bracero, O. L., Naidoo, M., Park, S. S., Schechner, Y., Schofield, R., Tripathi, S. N., Windwer, E., Wu, M.-T., Zhang, Q., Brauer, M., Rudich, Y., and Martin, R. V.: Elemental Characterization of Ambient Particulate Matter for a Globally Distributed Monitoring Network: Methodology and Implications, ACS EST Air, https://doi.org/10.1021/acsestair.3c00069, 2024.

Lyapustin, A., Wang, Y., Korkin, S., and Huang, D.: MODIS Collection 6 MAIAC algorithm, Atmospheric Measurement Techniques, 11, 5741–5765, https://doi.org/10.5194/amt-11-5741-2018, 2018.

Martin, R. V., Jacob, D. J., Yantosca, R. M., Chin, M., and Ginoux, P.: Global and regional decreases in tropospheric oxidants from photochemical effects of aerosols, Journal of Geophysical Research: Atmospheres, 108, https://doi.org/10.1029/2002jd002622, 2003.

Martin, R. V., Brauer, M., van Donkelaar, A., Shaddick, G., Narain, U., and Dey, S.: No one knows which city has the highest concentration of fine particulate matter, Atmospheric Environment: X, 3, https://doi.org/10.1016/j.aeaoa.2019.100040, 2019.

Martin, R. V., Eastham, S. D., Bindle, L., Lundgren, E. W., Clune, T. L., Keller, C. A., Downs, W., Zhang, D., Lucchesi, R. A., Sulprizio, M. P., Yantosca, R. M., Li, Y., Estrada, L., Putman, W. M., Auer, B. M., Trayanov, L., Pawson, S., and Jacob, D. J.: Improved Advection , Resolution , Performance , and Community Access in the New Generation (Version 13) of the High Performance GEOS-Chem Global Atmospheric Chemistry Model (GCHP), Geoscientific Model Development Discussions, 720, 1–30, https://doi.org/10.5194/gmd-2022-42, 2022.

McDuffie, E. E., Martin, R. V., Spadaro, J. V., Burnett, R., Smith, S. J., O'Rourke, P., Hammer, M. S., van Donkelaar, A., Bindle, L., Shah, V., Jaeglé, L., Luo, G., Yu, F., Adeniran, J. A., Lin, J., and Brauer, M.: Source sector and fuel contributions to ambient PM2.5 and attributable mortality across multiple spatial scales, Nature Communications, 12, 1–12, https://doi.org/10.1038/s41467-021-23853-y, 2021.

Meng, J., Martin, R. V., Ginoux, P., Hammer, M., Sulprizio, M. P., Ridley, D. A., and Van Donkelaar, A.: Grid-independent high-resolution dust emissions (v1.0) for chemical transport models: Application to GEOS-Chem (12.5.0), Geoscientific Model Development, 14, 4249–4260, https://doi.org/10.5194/gmd-14-4249-2021, 2021.

Miao, R., Chen, Q., Zheng, Y., Cheng, X., Sun, Y., Palmer, P. I., Shrivastava, M., Guo, J., Zhang, Q., Liu, Y., Tan, Z., Ma, X., Chen, S., Zeng, L., Lu, K., and Zhang, Y.: Model bias in simulating major chemical components of $PM_{2.5}$ in China, Atmospheric Chemistry and Physics, 20, 12265–12284, https://doi.org/10.5194/acp-20-12265-2020, 2020.

Nguyen, T. T. N., Pham, H. V., Lasko, K., Bui, M. T., Laffly, D., Jourdan, A., and Bui, H. Q.: Spatiotemporal analysis of ground and satellite-based aerosol for air quality assessment in the Southeast Asia region, Environmental Pollution, 255, 113106, https://doi.org/10.1016/j.envpol.2019.113106, 2019.

CEDS: https://www.pnnl.gov/projects/ceds, last access: 6 July 2024.

Pai, S. J., Heald, C. L., Pierce, J. R., Farina, S. C., Marais, E. A., Jimenez, J. L., Campuzano-Jost, P., Nault, B. A., Middlebrook, A. M., Coe, H., Shilling, J. E., Bahreini, R., Dingle, J. H., and Vu, K.: An evaluation of global organic aerosol schemes using airborne observations, Atmospheric Chemistry and Physics, 20, 2637–2665, https://doi.org/10.5194/acp-20-2637-2020, 2020.

Park, R. J., Jacob, D. J., Chin, M., and Martin, R. V.: Sources of carbonaceous aerosols over the United States and implications for natural visibility, Journal of Geophysical Research Atmospheres, 108, https://doi.org/10.1029/2002jd003190, 2003.

Philip, S., Martin, R. V., van Donkelaar, A., Lo, J. W.-H., Wang, Y., Chen, D., Zhang, L., Kasibhatla, P. S., Wang, S., Zhang, Q., Lu, Z., Streets, D. G., Bittman, S., and Macdonald, D. J.: Global Chemical Composition of Ambient Fine Particulate Matter for Exposure Assessment, Environ. Sci. Technol., 48, 13060–13068, https://doi.org/10.1021/es502965b, 2014a.

Philip, S., Martin, R. V., Pierce, J. R., Jimenez, J. L., Zhang, Q., Canagaratna, M. R., Spracklen, D. V., Nowlan, C. R., Lamsal, L. N., Cooper, M. J., and Krotkov, N. A.: Spatially and seasonally resolved estimate of the ratio of organic mass to organic carbon, Atmospheric Environment, 87, 34–40, https://doi.org/10.1016/j.atmosenv.2013.11.065, 2014b.

Philip, S., Martin, R. V., Snider, G., Weagle, C. L., Van Donkelaar, A., Brauer, M., Henze, D. K., Klimont, Z., Venkataraman, C., Guttikunda, S. K., and Zhang, Q.: Anthropogenic fugitive, combustion and industrial dust is a significant, underrepresented fine particulate matter source in global atmospheric models, Environmental Research Letters, 12, https://doi.org/10.1088/1748-9326/aa65a4, 2017.

735 Pinault, L., Tjepkema, M., Crouse, D. L., Weichenthal, S., van Donkelaar, A., Martin, R. V.,
736 Brauer, M., Chen, H., and Burnett, R. T.: Risk estimates of mortality attributed to low
737 concentrations of ambient fine particulate matter in the Canadian community health survey cohort,
738 Environmental Health, 15, 18, https://doi.org/10.1186/s12940-016-0111-6, 2016.

739 Prank, M., Sofiev, M., Tsyro, S., Hendriks, C., Semeena, V., Vazhappilly Francis, X., Butler, T.,
740 Denier van der Gon, H., Friedrich, R., Hendricks, J., Kong, X., Lawrence, M., Righi, M., Samaras,
741 Z., Sausen, R., Kukkonen, J., and Sokhi, R.: Evaluation of the performance of four chemical
742 transport models in predicting the aerosol chemical composition in Europe in 2005, Atmospheric
743 Chemistry and Physics, 16, 6041–6070, https://doi.org/10.5194/acp-16-6041-2016, 2016.

744 Sayer, A. M., Munchak, L. A., Hsu, N. C., Levy, R. C., Bettenhausen, C., and Jeong, M. J.: MODIS
745 Collection 6 aerosol products: Comparison between Aqua's e-Deep Blue, Dark Target, and
746 "merged" data sets, and usage recommendations, Journal of Geophysical Research: Atmospheres,
747 119, 13,965-13,989, https://doi.org/10.1002/2014JD022453, 2014.

748 Schubert, S. D., Rood, R. B., and Pfaendtner, J.: An Assimilated Dataset for Earth Science
749 Applications, Bulletin of the American Meteorological Society, 74, 2331–2342,
750 https://doi.org/10.1175/1520-0477(1993)074<2331:AADFES>2.0.CO;2, 1993.

751 Sha, T., Ma, X., Jia, H., Tian, R., Chang, Y., Cao, F., and Zhang, Y.: Aerosol chemical component:
752 Simulations with WRF-Chem and comparison with observations in Nanjing, Atmospheric
753 Environment, 218, 116982, https://doi.org/10.1016/j.atmosenv.2019.116982, 2019.

754 Shimadera, H., Hayami, H., Chatani, S., Morino, Y., Mori, Y., Morikawa, T., Yamaji, K., and
755 Ohara, T.: Sensitivity analyses of factors influencing CMAQ performance for fine particulate
756 nitrate, Journal of the Air & Waste Management Association, 64, 374–387,
757 https://doi.org/10.1080/10962247.2013.778919, 2014.

758 Snider, G., Weagle, C. L., Murdymootoo, K. K., Ring, A., Ritchie, Y., Stone, E., Walsh, A.,
759 Akoshile, C., Anh, N. X., Balasubramanian, R., Brook, J., Qonitan, F. D., Dong, J., Griffith, D.,
760 He, K., Holben, B. N., Kahn, R., Lagrosas, N., Lestari, P., Ma, Z., Misra, A., Norford, L. K., Quel,
761 E. J., Salam, A., Schichtel, B., Segev, L., Tripathi, S., Wang, C., Yu, C., Zhang, Q., Zhang, Y.,
762 Brauer, M., Cohen, A., Gibson, M. D., Liu, Y., Martins, J. V., Rudich, Y., and Martin, R. V.:
763 Variation in global chemical composition of PM2.5: emerging results from SPARTAN,
764 Atmospheric Chemistry and Physics, 16, 9629–9653, https://doi.org/10.5194/acp-16-9629-2016,
765 2016.

766 Travis, K. R., Crawford, J. H., Chen, G., Jordan, C. E., Nault, B. A., Kim, H., Jimenez, J. L.,
767 Campuzano-Jost, P., Dibb, J. E., Woo, J. H., Kim, Y., Zhai, S., Wang, X., McDuffie, E. E., Luo,
768 G., Yu, F., Kim, S., Simpson, I. J., Blake, D. R., Chang, L., and Kim, M. J.: Limitations in
769 representation of physical processes prevent successful simulation of PM2.5 during KORUS-AQ,
770 Atmospheric Chemistry and Physics, 22, 7933–7958, https://doi.org/10.5194/acp-22-7933-2022,
771 2022.

772 Wang, Q., Jacob, D. J., Spackman, J. R., Perring, A. E., Schwarz, J. P., Moteki, N., Marais, E. A.,
773 Ge, C., Wang, J., and Barrett, S. R. H.: Global budget and radiative forcing of black carbon aerosol:

774 Constraints from pole-to-pole (HIPPO) observations across the Pacific, Journal of Geophysical
775 Research, 119, 195–206, https://doi.org/10.1002/2013JD020824, 2014.

776 Wang, Y., Jacob, D. J., and Logan, J. A.: Global simulation of tropospheric O3-NOx-hydrocarbon
777 chemistry - 1. Model formulation, Journal of Geophysical Research: Atmospheres, 103, 10713–
778 10725, https://doi.org/10.1029/98jd00158, 1998.

779 Weagle, C. L., Snider, G., Li, C., Van Donkelaar, A., Philip, S., Bissonnette, P., Burke, J., Jackson,
780 J., Latimer, R., Stone, E., Abboud, I., Akoshile, C., Anh, N. X., Brook, J. R., Cohen, A., Dong, J.,
781 Gibson, M. D., Griffith, D., He, K. B., Holben, B. N., Kahn, R., Keller, C. A., Kim, J. S., Lagrosas,
782 N., Lestari, P., Khian, Y. L., Liu, Y., Marais, E. A., Martins, J. V., Misra, A., Muliane, U., Pratiwi,
783 R., Quel, E. J., Salam, A., Segev, L., Tripathi, S. N., Wang, C., Zhang, Q., Brauer, M., Rudich, Y.,
784 and Martin, R. V.: Global Sources of Fine Particulate Matter: Interpretation of PM2.5 Chemical
785 Composition Observed by SPARTAN using a Global Chemical Transport Model, Environmental
786 Science and Technology, 52, 11670–11681, https://doi.org/10.1021/acs.est.8b01658, 2018.

787 Weichenthal, S., Pinault, L., Christidis, T., Burnett, R. T., Brook, J. R., Chu, Y., Crouse, D. L.,
788 Erickson, A. C., Hystad, P., Li, C., Martin, R. V., Meng, J., Pappin, A. J., Tjepkema, M., van
789 Donkelaar, A., Weagle, C. L., and Brauer, M.: How low can you go? Air pollution affects mortality
790 at very low levels, Science Advances, 8, eabo3381, https://doi.org/10.1126/sciadv.abo3381, 2022.

791 Wendt, E. A., Ford, B., Cheeseman, M., Rosen, Z., Pierce, J. R., H. Jathar, S., L'Orange, C., Quinn,
792 C., Long, M., Mehaffy, J., D. Miller-Lionberg, D., H. Hagan, D., and Volckens, J.: A national
793 crowdsourced network of low-cost fine particulate matter and aerosol optical depth monitors:
794 results from the 2021 wildfire season in the United States, Environmental Science: Atmospheres,
795 3, 1563–1575, https://doi.org/10.1039/D3EA00086A, 2023.

796 Weng, H., Lin, J., Martin, R., Millet, D. B., Jaeglé, L., Ridley, D., Keller, C., Li, C., Du, M., and
797 Meng, J.: Global high-resolution emissions of soil NOx, sea salt aerosols, and biogenic volatile
798 organic compounds, Scientific Data, 7, 1–15, https://doi.org/10.1038/s41597-020-0488-5, 2020.

799 van der Werf, G. R., Randerson, J. T., Giglio, L., Van Leeuwen, T. T., Chen, Y., Rogers, B. M.,
800 Mu, M., Van Marle, M. J. E., Morton, D. C., Collatz, G. J., Yokelson, R. J., and Kasibhatla, P. S.:
801 Global fire emissions estimates during 1997-2016, Earth System Science Data, 9, 697–720,
802 https://doi.org/10.5194/essd-9-697-2017, 2017.

803 White, W. H., Trzepla, K., Hyslop, N. P., and Schichtel, B. A.: A critical review of filter
804 transmittance measurements for aerosol light absorption, and de novo calibration for a decade of
805 monitoring on PTFE membranes, Aerosol Science and Technology, 50, 984–1002,
806 https://doi.org/10.1080/02786826.2016.1211615, 2016.

807 Xin, J., Zhang, Q., Wang, L., Gong, C., Wang, Y., Liu, Z., and Gao, W.: The empirical relationship
808 between the PM2.5 concentration and aerosol optical depth over the background of North China
809 from 2009 to 2011, Atmospheric Research, 138, 179–188,
810 https://doi.org/10.1016/j.atmosres.2013.11.001, 2014.

Yang, Q., Yuan, Q., Yue, L., Li, T., Shen, H., and Zhang, L.: The relationships between PM2.5 and aerosol optical depth (AOD) in mainland China: About and behind the spatio-temporal variations, Environmental Pollution, 248, 526–535, https://doi.org/10.1016/j.envpol.2019.02.071, 2019.

Zhai, S., Jacob, D., Brewer, J., Li, K., Moch, J., Kim, J., Lee, S., Lim, H., Lee, H. C., Kuk, S. K., Park, R., Jeong, J., Wang, X., Liu, P., Luo, G., Yu, F., Meng, J., Martin, R., Travis, K., Hair, J., Anderson, B., Dibb, J., Jimenez, J., Campuzano-Jost, P., Nault, B., Woo, J.-H., Kim, Y., Zhang, Q., and Liao, H.: Interpretation of geostationary satellite aerosol optical depth (AOD) over East Asia in relation to fine particulate matter (PM2.5): insights from the KORUS-AQ aircraft campaign and seasonality, Atmospheric Chemistry and Physics, 1–23, https://doi.org/10.5194/acp-2021-413, 2021.

Zhang, H., Hoff, R. M., and Engel-Cox, J. A.: The relation between moderate resolution imaging spectroradiometer (MODIS) aerosol optical depth and PM2.5 over the United States: A geographical comparison by U.S. Environmental Protection Agency regions, Journal of the Air and Waste Management Association, 59, 1358–1369, https://doi.org/10.3155/1047-3289.59.11.1358, 2009.

Zhang, L., Jacob, D. J., Knipping, E. M., Kumar, N., Munger, J. W., Carouge, C. C., Van Donkelaar, A., Wang, Y. X., and Chen, D.: Nitrogen deposition to the United States: Distribution, sources, and processes, Atmospheric Chemistry and Physics, 12, 4539–4554, https://doi.org/10.5194/ACP-12-4539-2012, 2012.

Zhang, L., Kok, J. F., Henze, D. K., Li, Q., and Zhao, C.: Improving simulations of fine dust surface concentrations over the western United States by optimizing the particle size distribution, Geophysical Research Letters, 40, 3270–3275, https://doi.org/10.1002/grl.50591, 2013.

Zhao, B., Jiang, J. H., Diner, D. J., Su, H., Gu, Y., Liou, K.-N., Jiang, Z., Huang, L., Takano, Y., Fan, X., and Omar, A. H.: Intra-annual variations of regional aerosol optical depth, vertical distribution, and particle types from multiple satellite and ground-based observational datasets, Atmospheric Chemistry and Physics, 18, 11247–11260, https://doi.org/10.5194/acp-18-11247-2018, 2018.

Zhu, H., Martin, R. V., Croft, B., Zhai, S., Li, C., Bindle, L., Pierce, J. R., Chang, R. Y. W., Anderson, B. E., Ziemba, L. D., Hair, J. W., Ferrare, R. A., Hostetler, C. A., Singh, I., Chatterjee, D., Jimenez, J. L., Campuzano-Jost, P., Nault, B. A., Dibb, J. E., Schwarz, J. S., and Weinheimer, A.: Parameterization of size of organic and secondary inorganic aerosol for efficient representation of global aerosol optical properties, Atmospheric Chemistry and Physics, 23, 5023–5042, https://doi.org/10.5194/ACP-23-5023-2023, 2023.